Coordination Chemistry Reviews 277–278 (2014) 44–68

Contents lists available at ScienceDirect

Coordination Chemistry Reviews

journal homepage: www.elsevier.com/locate/ccr

Review

Recent experimental and theoretical developments in time-resolved X-ray spectroscopies

C.J. Milne [b], T.J. Penfold [a,b], M. Chergui [a,*]

[a] École Polytechnique Fédérale de Lausanne, Laboratoire de spectroscopie ultrarapide, ISIC, FSB-BSP, CH-1015 Lausanne, Switzerland
[b] SwissFEL, Paul Scherrer Institute, CH-5232 Villigen, Switzerland

Contents

ARTICLE INFO

Article history:
Received 27 November 2013
Received in revised form 3 February 2014
Accepted 3 February 2014
Available online 12 March 2014

ABSTRACT

Capturing the evolving geometric and electronic structure in the course of a chemical reaction or biological process is the principal aim of time-resolved X-ray spectroscopies. Recent technological and methodological improvements, such as high repetition rate lasers and femtosecond laser-electron slicing have made this a reality. The advent of X-ray free electron lasers introduces a paradigm shift in terms of the temporal resolution of X-ray spectroscopies, and offer exciting possibilities for time-resolved second-order

* Corresponding author. Tel.: +41 21 693 0457/0447; fax: +41 21 693 0365.
E-mail address: majed.chergui@epfl.ch (M. Chergui).

http://dx.doi.org/10.1016/j.ccr.2014.02.013

Keywords:
Time-resolved X-ray spectroscopy
Femtosecond
X-ray free electron laser
Nonadiabatic
Non-linear

X-ray spectroscopies and non-linear X-ray experiments. In parallel, the improved data quality is making it increasingly important to accurately simulate the fine spectroscopic details. This has been the driving force for new theoretical methods permitting a detailed interpretation of the spectra in terms of the geometrical and electronic properties of the system. In this contribution, we discuss recent experimental and theoretical developments in ultrafast X-ray absorption spectroscopies (XAS) and explore the new opportunities they offer.

1. Introduction

Ultrafast studies emerged with the implementation of femtosecond–picosecond linear and non-linear optical spectroscopies [1–3] and had a huge impact on our understanding of chemical reactions, biological functions and phase transitions in materials owing to their ability to probe, in real-time, the nuclear motion within these different types of systems. However, for systems of more than two atoms the link between the optical domain spectroscopic observables and the molecular structure is ambiguous and therefore from the early days of ultrafast spectroscopy much effort was invested to develop methods that achieve both high temporal (on the femtosecond time scale) and spatial (on the order on tenths of an angström) resolution. Towards this goal, various groups adopted diffraction methods based on the use of ultrashort pulses of X-rays [4–6] or electrons [7–10], while others opted for time-resolved X-ray absorption spectroscopy (XAS) [11–17].

XAS is particularly attractive because of its ability to deliver electronic structure as well as geometric information. For the implementation of time-resolved XAS, third generation light sources (i.e. storage rings that generate synchrotron radiation) are most suited because of their wide tuneability, stability and high photon flux. However, the physics of storage rings limits the X-ray pulse duration to 50–100 ps. Nevertheless, several exciting results were gathered on a wide variety of chemical systems [12,13,18–33] and materials [34–37]. The temporal limitation of storage rings has been overcome by the laser-electron slicing scheme [38–41] and the so-called *low-alpha* modes [42,43], albeit at the sacrifice of photon flux. The slicing scheme in particular has made it possible to demonstrate femtosecond XAS of photoexcited molecular species in solution [44–46]. In parallel, the advent of X-ray free electron lasers (X-FELs) is starting to yield the first results in ultrafast XAS [47], which promises to revolutionise the field.

For achieving a full understanding of an experimental spectrum, theoretical simulations are essential. Such analysis has usually been performed using multiple scattering (MS) theory, within the limits of the muffin-tin (MT) potential [48] or using multiplet theory [49,50]. However, while these approaches have provided significant insight into the origin of both static and time-resolved spectra [23,25], the increasing information available from time-resolved spectroscopies means that one must go beyond the present approximations and, in an *ab initio* manner, include the influence of strong electron correlation [51–56], nuclear dynamics beyond the Born-Oppenheimer approximation and non-linear effects [57].

In this contribution, we review some of the most recent advances in both experimental and theoretical approaches for time-resolved XAS. We broaden the scope by discussing some of the new opportunities for time domain core-level spectroscopies such as X-ray emission spectroscopy (XES), and Resonant inelastic X-ray scattering (RIXS) and the potential impact of femtosecond temporal resolution and high fluxes provided by the X-FELs. This review is organised in the following way: In the first section, we recall the basic aspects of core-level spectroscopies. This is followed by a discussion on X-ray sources used for such experiments. A detailed summary of the experimental developments is then presented followed by an examination of theoretical developments.

2. X-ray spectroscopies

2.1. X-ray absorption spectroscopy

An X-ray absorption spectrum (XAS) is characterised by absorption edges, which reflect the ionisation threshold of the different core orbitals, shown schematically in Fig. 1. The physical processes and information content have been presented in detail in a number of books and review papers [58,59,48,50] and we will therefore not discuss them in detail here. Briefly, for a particular edge, an electron is initially excited to empty or partially filled orbitals just below the ionisation potential (IP) yielding information about the unoccupied density of states. The energy of the absorption edge provides information about the oxidation and spin state of the absorbing atom. Just above the edge (<50 eV), in the X-ray Absorption Near-Edge Structure (XANES) region, the low photoelectron energy (i.e. long de Broglie wavelength) implies that the photoelectron undergoes multiple scattering (MS) events. XANES therefore contains information about the three-dimensional structure around the absorbing atom, i.e. bond distances and bond angles. At higher energies, in the Extended X-ray Absorption Fine Structure (EXAFS) region, single scattering (SS) events usually dominate, as the scattering cross section of the photoelectron decreases increasing energy. This region delivers information about coordination numbers and

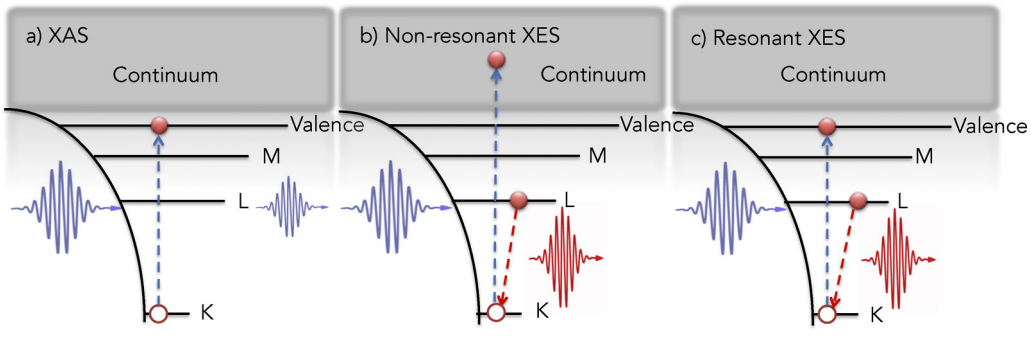

Fig. 1. Schematic energy level diagrams of XAS (a), non-resonant XES (b) and resonant XES (c).

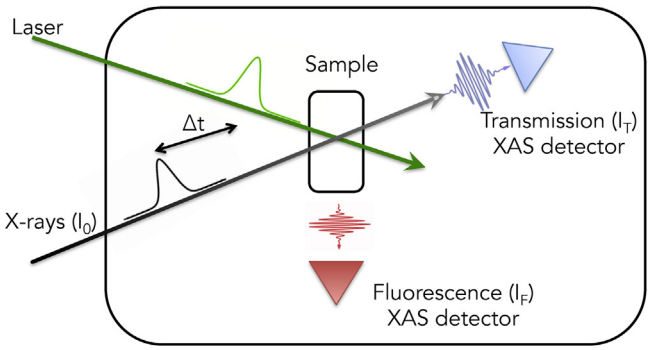

Fig. 2. Sketch of a typical time-resolved XAS setup for the study of liquid samples. The continuously-refreshed sample can be a flow capillary, a flow-cell, or a high speed liquid jet. Δt is the time-delay between the laser pump and X-ray probe pulses.

bond distances of the first coordination shell around the absorbing atom.

The simplest and most common method of measuring the X-ray absorption coefficient is X-ray transmission, shown schematically in Fig. 2. Using a tuneable monochromatic X-ray beam ($\Delta\Omega/\Omega \sim 0.015\,\%$) both the transmitted ($I_T$) and incident ($I_0$) X-ray signals are measured as a function of incident photon energy. The X-ray linear absorption coefficient $\mu(\Omega)$, at a particular incident photon energy Ω is then derived from the Beer–Lambert law:

$$A(\Omega) = \mu(\Omega) \cdot d = \ln\left(\frac{I_0}{I_T}\right), \tag{1}$$

where d represents the sample thickness. In principle, $\mu(\Omega)$ refers to the total absorption coefficient of the sample, which includes not only the absorbing atom, but also the environment in which it is contained, along with Compton scattering. The absorption coefficient is calculated using Fermi's Golden Rule:

$$\mu(\Omega) \sim \sum_f |\langle f|\hat{H}_{\text{int}}|i\rangle|^2 \times \frac{\Gamma_f/2\pi}{(E_f - E_i - \hbar\Omega)^2 + \Gamma_f^2/4} \tag{2}$$

describing the transition from an initial state (i) with energy E_i to a final state (f) with energy E_f. $\hat{H}_{\text{int}}$ is the interaction Hamiltonian, typically within the dipole or dipole + quadrupole approximation, $\hbar\Omega$ is the energy of the incident photons and Γ_f is the core-hole lifetime broadening.

When extended to the time-domain as shown schematically in Fig. 2, the XAS signal at a particular X-ray energy and pump-probe time delay (Δt) is recorded twice, alternating between the signal from the excited sample (pumped) and that from the unexcited sample (unpumped). A zero measurement is also made by reading the detector signal in the gap where no X-rays are present, which is then subtracted off the corresponding X-ray signal to compensate for any drifts over time of the data acquisition baseline. The transient spectrum is then expressed as the difference between the pumped (excited) minus the unpumped (ground state):

$$\Delta I(\Omega, t) = f \cdot [\Phi(t) I_{pumped}(\Omega) - I_{unpumped}(\Omega)], \tag{3}$$

where f is the photolysis yield and $\Phi(t)$ represents the quantum yield of the product, whose time dependence reflects decay processes. This general methodology also applies for the second-order spectroscopies discussed in the proceeding section.

2.2. Second-order X-ray spectroscopies

X-ray absorption spectroscopy provides insight into the unoccupied valence orbital of a particular system and, through the above ionisation resonances, insight into the geometric structure around the absorbing atom. However, the advent of intense X-ray sources and high-resolution detectors is making it possible to perform X-ray emission (XES) or X-ray Raman spectroscopy. In this case the incident photon is absorbed and the emitted or scattered photon is detected meaning that such spectroscopies must be treated within second-order perturbation theory [60].

These second-order spectroscopies (also called photon-in/photon-out [61,62]) have spawned a whole range of approaches, and while the yields are much smaller than signals from traditional transmission XAS, they are able to probe both the unoccupied and occupied molecular orbitals, obtain soft X-ray L-edge, M-edge and UV–vis excitations using hard X-rays, perform site selective and/or range-extended EXAFS [63–65] and record high-resolution spectra proportional to the X-ray absorption spectrum. Importantly, the low scattering cross sections of these spectroscopies has so far restricted their use in time-resolved studies, however the increased available photon flux at 3rd-generation storage rings using high repetition rate schemes or of the X-FELs means that time-resolved second-order spectroscopies are emerging as powerful tools in coordination chemistry.

For spectroscopies based upon the detection of scattered (fluorescent) photons, the spectra are represented using the Kramers–Heisenberg equation [66–68]:

$$F(\Omega, \omega) = \sum_f \left| \sum_n \frac{\langle f|\hat{H}_{\text{int}}|n\rangle\langle n|\hat{H}_{\text{int}}|i\rangle}{E_i - E_n - \hbar\Omega - i\frac{\Gamma_n}{2}} \right|^2 \times \frac{\Gamma_f/2\pi}{(E_i - E_f + \hbar\Omega - \hbar\omega)^2 + \Gamma_f^2/4} \tag{4}$$

where $\hbar\Omega$ and $\hbar\omega$ are the incident and emitted photons, respectively and E_i, E_n, E_f are the energies of the initial, intermediate and final states. Γ_n and Γ_f are the lifetime broadening associated with the intermediate and final states.

Eq. 4 describes the absorption of a photon, forming an intermediate state n from the ground state i, before it decays into a final state f. This second-order process can be described as absorption and emission processes that are coherently coupled. One effect of this coupling is that interference between different intermediate states can alter the spectral weights. However, in the case of hard X-rays, these are generally small and the interference terms can be neglected. Under this approximation Eq. 4 becomes:

$$F(\Omega, \omega) = \sum_f \sum_n \left| \frac{\langle f|\hat{H}_{\text{int}}|n\rangle\langle n|\hat{H}_{\text{int}}|i\rangle}{E_i - E_n + \hbar\Omega - i\frac{\Gamma_n}{2}} \right|^2 \times \frac{\Gamma_f/2\pi}{(E_i - E_f + \hbar\Omega - \hbar\omega)^2 + \Gamma_f^2/4} \tag{5}$$

$$= \sum_f \sum_n \frac{\langle f|\hat{H}_{\text{int}}|n\rangle^2\langle n|\hat{H}_{\text{int}}|i\rangle^2}{(E_i - E_n + \hbar\Omega)^2 + \Gamma_n^2/4} \times \frac{\Gamma_f/2\pi}{(E_i - E_f + \hbar\Omega - \hbar\omega)^2 + \Gamma_f^2/4} \tag{6}$$

This describes a non-coherent process in which the absorption matrix elements from initial state i to intermediate state n is weighted by the emission matrix element. An example of this is total fluorescence yield (TFY) spectroscopy, in which the total fluorescence from the sample is collected, without energy resolution as a function of the incident photon energy [69,70]. This approach can be advantageous when the signal of interest contributes only

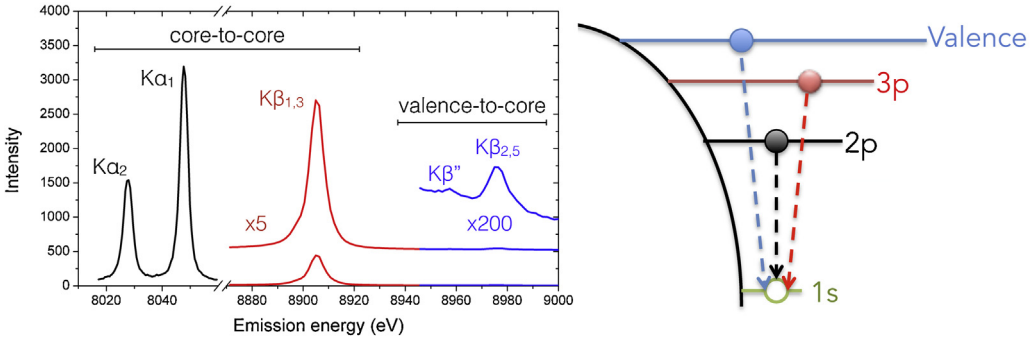

Fig. 3. The K shell emission lines in CuO (right) [80] and a schematic (left) of the transitions. The strongest lines are the K_{α_1} and K_{α_2}, which correspond to transitions from the $2p_{3/2}$ and $2p_{1/2}$ levels, respectively. The $K\beta_{1,3}$ lines are $3p \rightarrow 1s$ transitions and at higher emission energy the $K\beta_{2,5}/K\beta''$ transitions form the so-called valence-to-core emission lines.

a small fraction to the total absorption, or when the sample transmission is very large.

2.2.1. Non-resonant X-ray emission

X-ray emission probes the photons emitted by an electron refilling a core hole created by the incident photon, and therefore it is able to probe the electronic structure of the occupied orbitals. For non-resonant X-ray emission (NXES), the incident photon energy is much greater than the Fermi energy and a core electron is ejected into the continuum, as shown schematically in Fig. 1b. In this case the spectral weights are largely independent of the incident photon energy and the lifetime broadening of the spectrum corresponds to $\Gamma_n+\Gamma_f$ [71].

Fig. 3 shows the K emission spectrum of CuO, i.e. the fluorescence after creation of a hole in the Cu 1s orbital, which is characterised by a number of distinct resonances. The strongest lines are the $K\alpha_1$ and $K\alpha_2$, which correspond to transitions from the $2p_{3/2}$ and $2p_{1/2}$ levels, respectively. These, so-called core-to-core transitions are commonly employed to retrieve fluorescence yield XAS (see Section 2.2.3). At higher emission energies lie the $3p \rightarrow 1s$ transitions which form the $K\beta_{1,3}$ lines. These are nearly an order of magnitude weaker than the K_α transitions. Higher still are the $K\beta_{2,5}/K\beta''$ transitions, which form the so-called valence-to-core emission lines. They involve the relaxation of the valence electrons into the core-hole, and are much weaker due to a poorer overlap of initial and final wavefunctions. These transitions provide strong sensitivity to the chemical environment of the scattering atom, and in particular the ligand orbitals and bond distances [72–79] and therefore their implementation in time-domain experiments will yield important information about the changes of the valence electron density in an ultrafast chemical process.

2.2.2. Resonant X-ray emission

If the incident photon energy is tuned below the ionisation potential to the energy of an unoccupied orbital as shown in Fig. 1c, resonant X-ray emission (RXES) occurs. Compared with NXES, the spectral shape and intensity of RXES spectra are dependent on the nature of the transition that is excited (pre-edge, white line, etc.) [81,67,82–84].

If the incoming photon resonantly excites a core electron into an unoccupied level, which then decays back to its initial core state, the emitted photon will have the same energy as the incoming one (although different polarisation and wave vector) yielding resonant elastic X-ray scattering [85,86]. In this case the total scattering intensity must also incorporate second-order absorption and emission processes (Eq. (4)), responsible for the so-called anomalous scattering amplitude [86]. This introduces abrupt changes to the intensity of the diffraction peaks around resonances within the material. This approach can be seen as combining XAS and X-ray diffraction in a single experiment, where the X-ray direction yields spatial information, while the spectroscopic part, through the anomalous scattering amplitude, provides sensitivity to the electronic states of the system and in particular to charge, orbital and spin ordering phenomena [87]. This approach requires both long-range order within the sample and precise control over the macroscopic sample orientation with respect to the incident X-ray beam, and consequently is most widely used for problems in condensed matter physics.

Alternatively if the incoming and outgoing photon energies are not equal, an energy transfer to the system occurs [89–93]. This is called both resonant X-ray emission spectroscopy (RXES) [62] and resonant inelastic X-ray scattering (RIXS) in the literature. We will use the term RIXS to refer to such measurements in the following sections. In RIXS, both the incident and emitted (or energy transfer) photon energies are resolved and plotted on a two dimensional (2D) correlation plot. However, RIXS may also provide direct insight into the momentum dependence of the transitions. By recording both the energy and momentum of the emitted photons (momentum-resolved RIXS), it is possible to obtain information about the spatial dispersion of the fundamental excitations [68,50,67,94]. Such methodology has been widely used to study charge transfer, *dd* transitions [95], magnons [96] and phonon excitations [97].

Fig. 4 shows the $2p_{3/2}$–$3d_{5/2}$ RIXS plane of the photocatalytically active di-platinum complex $[Pt_2(P_2O_5H_2)_4]^{4-}$ (PtPOP) measured in solution in the two most commonly used presentation formats: *XAS vs XES* and *XAS vs Energy transfer*. This measurement was performed by scanning the incident X-ray energy through the Pt L_3 X-ray absorption edge (11.56 keV) and using a von Hamos geometry dispersive X-ray spectrometer [88] to measure the $L\alpha_1$ X-ray emission (9.44 keV). By resolving both the incident and emitted photon energies, this approach is able to simultaneously measure the occupied and unoccupied density of states around the resonant core excitation. In addition, the energy transferred corresponds to elementary excitation of the final state within the material, which can include such low-energy collective excitations as phonons or plasmons in the solid state [67], and charge-transfer or ligand-field excitations in molecular systems [52,98].

2.2.3. High-resolution X-ray absorption spectra

Eq. (5) shows that when interference effects are neglected, the signal is related to the product of the squared absorption and emission spectra and provides the opportunity to obtain the absorption spectrum by monitoring emission processes. While this does not always hold (see Ref. [99]), it does in the case of hard X-ray spectroscopies. For achieving a high-resolution spectrum the most commonly adopted approach is high energy resolution fluorescence detection (HERFD) [93]. Here, the spectrum is recorded at a

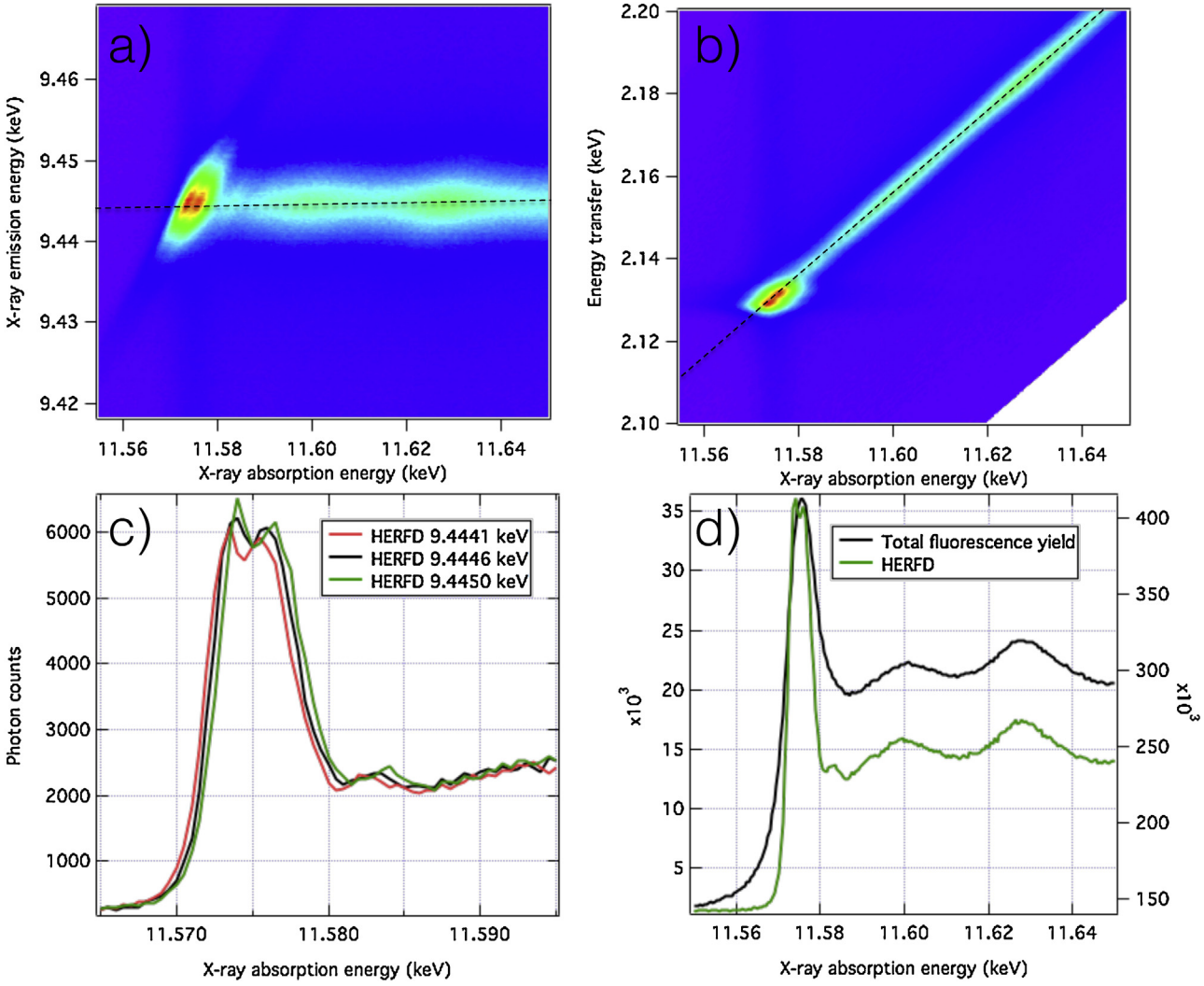

Fig. 4. RIXS measurements of the di-platinum complex $[Pt_2(P_2O_5H_2)_4]^{4-}$ measured in solution around the Pt L_3-edge using a dispersive von Hamos spectrometer [88]. (a) and (b) present the $2p_{3/2}$–$3d_{5/2}$ RIXS plane as *XAS vs XES* and *XAS vs Energy transfer* plots, respectively, where Energy transfer = XAS − XES. (c) shows high-energy resolution fluorescence detection (HERFD) signals at three X-ray emission energies, corresponding to horizontal slices in (a) and diagonal slices in (b). Note the sensitivity of the HERFD signal to the chosen emission energy. (d) Comparison between the total fluorescence yield (TFY) and HERFD signals, illustrating the increased energy resolution possible with the HERFD technique.

fixed emission energy as a function of incident photon energy. This corresponds to a horizontal line in Fig. 4a, where the signal is plotted as incident vs outgoing photon energies, and a diagonal line in Fig. 4b where the outgoing energy is plotted as a function of energy transferred to the system ($\Omega - \omega$). In this case the spectral width is dominated by the lifetime broadening of the final state hole and is therefore sharper than a XAS spectrum recorded in transmission or total fluorescence yield mode [100–102,89,82,103]. Although, as shown in Eq. (6), both Γ_f and Γ_i contribute to the band width of the HERFD spectrum, when the outgoing photons are detected at a constant emission energy and $\Gamma_i \gg \Gamma_f$, the broadening of the former (Γ_i) has little effect on the overall width. This is shown schematically in Refs. [100,104].

Fig. 4d shows a comparison between the TFY and HERFD signals measured on PtPOP. The HERFD signal clearly shows that the primary XAS peak at 11.575 keV is composed of two transitions, while the shoulder on the blue side of the main peak is a discrete transition, allowing a more accurate comparison to theoretical calculations [105]. The drawback of measuring a single emission energy is demonstrated in Fig. 4c where the HERFD signal measured at three different emission energies is presented. By changing the emission energy by small amounts (~0.5 eV), the HERFD signal shifts in energy and introduces intensity changes in the relative features of the spectrum, meaning that care must be taken when assigning importance to absolute energies and intensities in a HERFD spectrum. In relation to time-resolved studies, for such spectra it is not known *a priori* if the initial excitation will cause a shift in the emission lines or a change in intensity of the emission spectrum. Thus recording only the constant emission at a particular energy can distort the obtained spectrum. It is therefore always desirable to measure the full RIXS plane. This can also apply in the case of ground state spectra [82].

Finally, a new approach for achieving lifetime-broadening suppressed XAS spectra is the high resolution off-resonant spectroscopy (HEROS) [106,88,107]. This approach can be thought of as analogous to HERFD, however crucially the incident pulse energy is below the lowest transition energy as depicted in Fig. 5. In this case, the transitions only occur by virtue of the effect of the core-hole lifetime broadening (i.e. the Heisenberg uncertainty principle). This effect was first observed in Ref. [108] and later theoretically explained [109], however the small cross-sections ($\sigma_{HEROS}/\sigma_{ABS} \sim 10^{-8}$ vs $\sigma_{RIXS}/\sigma_{ABS} \sim 10^{-3}$) limited its use until sufficient photon fluxes could be achieved. Regarding both static and time-resolved measurements, its main advantage is that when

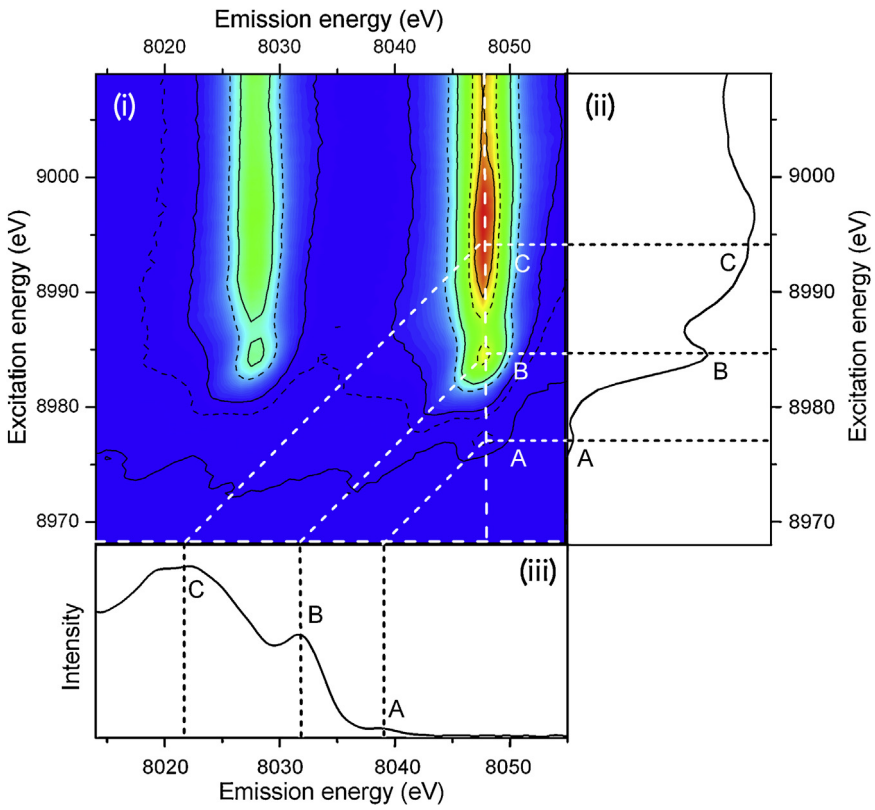

Fig. 5. (i) A schematic RIXS plane of CuO, showing the energy cuts corresponding to a HERFD (ii) and HEROS (iii) spectra. The A, B, and C labels correspond to the primary features of the XANES spectrum. The HERFD spectrum was measured at the peak of the $K\alpha_1$ emission signal (8047 eV) and the HEROS spectrum was measured at an incident energy of 8968 eV.

Figure courtesy of J. Szlachetko.

combined with a dispersive spectrometer [106,88,107], it becomes possible to obtain a XANES spectrum in a single measurement.

3. Sources of X-ray pulses

The past 30 years witnessed rapid development in both the peak brilliance and temporal resolution of X-ray sources, making it possible to perform experiments that only a few short decades earlier were inconceivable. X-ray absorption and second-order spectroscopies are now routine experimental techniques, capable of providing unparalleled electronic and structural information on a wide variety of systems. With the continuing improvement in X-ray sources, more and more flux-demanding measurements are achievable.

For time-resolved XAS the requirement for wide tuneability, stability and high photon flux made third generation light sources the most suited, despite the limitations to temporal resolution. Consequently, although able to achieve femtosecond X-ray pulses, table-top laser plasma sources [110,111] which are isotropic, of limited energy tunability and unstable from pulse-to-pulse have been limited to X-ray diffraction [112,5,113–116], although ultrafast XAS with them has also been demonstrated [117,118] and progress continues [119–121]. Therefore although these types of sources provide promise that the goal of a table-top X-ray free electron laser will one day be possible [122], they are still very much in the development phase and will not be discussed further.

3.1. High-harmonic generation sources

A recent technique that has attracted significant attention is high-harmonic generation (HHG) where an ultrashort laser pulse is focused into a gas jet, resulting in the emission of high energy photons [123–125]. This technique produces photons in the soft X-ray (200–1000 eV) and vacuum-ultraviolet (VUV) range (10–200 eV). The soft X-ray pulses can contain 10^{14} photons per second in a 1% bandwidth and can achieve sub-femtosecond temporal resolution [126]. HHG sources for time-resolved core-level absorption spectroscopy are increasingly being used in the VUV–XUV range for studies in the gas phase [127], liquids [128,129], and in solids [130,131].

3.2. Storage rings

Storage rings, which are also called synchrotrons, provide an intense source of high photon energy synchrotron radiation, making them ideal for performing X-ray spectroscopy [132]. In general terms storage rings produce high-energy photons by passing relativistic electrons through strong magnetic fields, forcing them to change direction. The acceleration results in the emission of electromagnetic radiation. The magnetic fields can be applied using a variety of devices including bending magnets, super-conducting bending magnets, wigglers, and undulators [133]. From a user perspective each of them has different characteristics and results in different X-ray sources for experiments.

Bending magnets generate a broad spectrum of photons, which extends out to the X-ray regime. The maximum X-ray flux in a bending magnet X-ray spectrum depends on the magnetic field strength of the magnet, the electron energy in the storage ring and the collection angle in the horizontally divergent beam. Undulators and wigglers consist of periodic arrays of permanent magnets, which force the electrons into an oscillatory trajectory as they pass through them. The result is a well collimated, spatially intense beam of X-rays. In general undulator beamlines produce

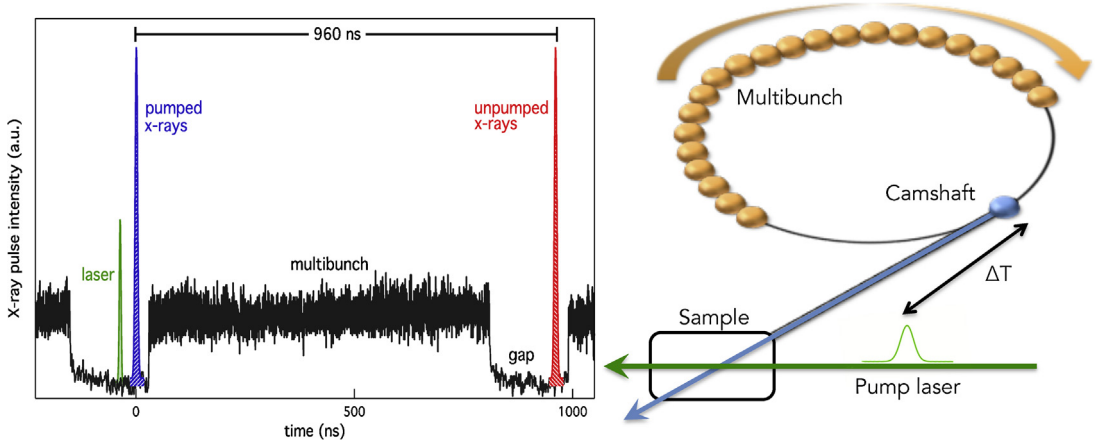

Fig. 6. Left: Plot of the X-ray fill pattern at the Swiss Light Source showing the isolated 'camshaft' pulse, the photo excitation laser pulse, the multibunch pulse train, and the ion-clearing gap. Right: Schematic of the X-ray fill pattern on the circular structure of the storage ring.

the highest spectral brilliance, with average photon fluxes exceeding 10^{12} photons/s. These so-called insertion devices also generate higher-order harmonic photons, which allows them to be used at higher photon energies, albeit with a loss in X-ray flux.

At an X-ray spectroscopy beamline, the X-ray photons are generally monochromatised using a crystal monochromator to a $\Delta E/E$ bandwidth of 0.01–0.03% [134]. This energy resolution is on the order of an eV in the hard X-ray regime, which is less than the typical core hole lifetime broadening in an X-ray spectrum. It is possible to use higher diffraction orders from the monochromator crystals, allowing higher energy resolution measurements for techniques such as momentum-resolved RIXS [67], where the scattering direction of the X-ray photon is also resolved, or Inelastic X-ray Scattering (IXS) [135]. The monochromatic X-rays can then be focused onto the sample using reflective achromatic X-ray optics, such as Kirkpatrick-Baez (KB) mirrors [136,137]. Another approach is energy dispersive XAS (EDXAS) where one uses an incident polychromatic beam, which is then either dispersed after the sample [138,139] or focussed using a curved crystal onto the sample, resulting in a spatially dispersed spectrum after the sample [140]. Both of these dispersive XAS techniques have also been used for time-resolved measurements [141,142], with the primary constraints being that only a transmission XAS measurement is possible and a two-dimensional detector is required.

The fill pattern of the electrons within the storage ring determines the time structure of the X-ray pulses. This consists of electron bunches separated by a few nanoseconds, with an entire revolution of the ring taking hundreds of nanoseconds to microseconds depending on the size of the storage ring (see Fig. 6). When a slow detector is used, the X-ray flux appears as a continuous stream of photons. By reading out the detector on timescales of milliseconds or seconds, the evolution of a sample can be recorded. If a faster detector is used the individual X-ray pulses can be observed (see Fig. 6), which allows the experiment to monitor sample evolution on much faster timescales. If the X-ray pulses are to be used in a pump-probe experiment, where the sample is initially excited using an ultrashort laser pulse and then subsequently probed after some adjustable time delay, it is necessary to isolate the X-rays from a single X-ray pulse. This can either be done using very fast detectors with sub-ns time resolution, or by taking advantage of the ability of storage rings to control the electron fill pattern within the storage ring. An example of such an approach is shown in Fig. 6 where the Swiss Light Source uses a 500 MHz radio-frequency source as the fundamental structure for its fill pattern. Bunches 1–400 are filled with 1 mA of electrons, and bunches 401–480 are left unfilled as an ion-clearing gap. An isolated bunch, sometimes called the camshaft, can be placed into this gap. This allows detectors with a time resolution of 10–20 ns to isolate the X-rays from the isolated bunch. The result is that measurements can then be performed where the time resolution is limited to the pulse duration of the isolated bunch, which is usually $\leq$100 ps [24,143,41]. This means that by judicious choice of detectors, X-ray spectroscopy measurements at storage rings are capable of covering an extremely broad range of timescales, from tens of picoseconds out to seconds and beyond [144].

3.3. X-ray free electron lasers

The recent development of X-FELs has revolutionised the field of ultrafast X-ray techniques [145–147]. These sources consist of a high-energy (GeV) electron bunch injected into a series of undulators that are hundreds of metres long. The oscillation of the electrons in the initial part of the undulators causes radiation to be emitted, as in a 3rd-generation storage ring. As the radiation and electrons co-propagate the radiation field builds up and the electrons start to interact with the radiation, causing a micro-bunch structure to appear with the wavelength of the radiation. This is represented pictorially in Fig. 7. This micro-bunch structure radiates coherent X-ray photons, the intensity of which builds up exponentially in a process called self-amplified spontaneous emission (SASE) until saturation is reached. The intensity increase is expressed as [148]:

$$I = I_0\, exp(Ax) \tag{7}$$

where x is the undulator length and A is a constant. The result is an intense, spatially coherent beam of femtosecond X-ray pulses, which can be used for experiments [149]. This high spatial

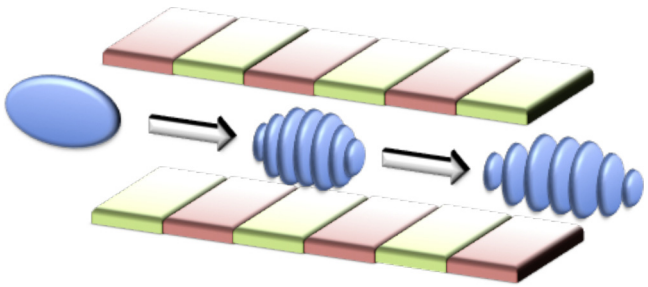

Fig. 7. Schematic of microbunching: as the electron bunch traverses the undulator or wiggler, microbunches are formed, due to the interaction between the travelling electrons and the previously emitted waves.

coherence reflects the strong correlation between the phases of the pulse at different points transverse to the direction of propagation, i.e. how uniform the phase of the wave front is. The effect of this high spatial coherence will be most noticeable in diffraction and imaging experiments [150–157]. Besides spatial coherence [158], temporal coherence is also important. This describes the correlation between the phases of the pulse at different points along the direction of propagation. For X-FELs the temporal coherence length is low due to the fact that the pulses contain more than a single frequency [149,159,160].

The FLASH VUV-soft X-ray free electron laser located at DESY in Hamburg has been the prototype for this kind of facility since it started user operation in mid-2005 [161–163]. It was soon followed in 2009 by the Linac Coherent Light Source (Stanford, CA, U.S.A.), which was the first hard X-ray free electron laser to come into operation [164]. LCLS now operates both in the soft and hard X-ray regimes, with experimental stations dedicated to various fields of research [165–169]. Recently the SACLA X-FEL facility at SPring-8 in Japan [170–172] and the FERMI@Elettra seeded VUV-soft X-ray FEL [173,174] also began operation, and several X-FEL projects are under construction worldwide, including machines in Germany [175], Korea [176,177], and Switzerland [178,179].

The primary feature of an X-FEL is the enormous number of photons/pulse (10^{11}–10^{12}) in a 10–100 fs pulse, or even sub-fs duration [180]. This makes their peak brilliance unparalleled. Both SACLA and LCLS operate at repetition rates of 100–120 Hz, which makes their average X-ray flux similar to that of 3rd-generation storage rings. However, because of the spontaneous nature of the SASE process, the radiation generated by X-FELs has a large variance in pulse energy (photon flux), photon energy (X-ray spectrum), and pulse arrival time large pulse-to-pulse fluctuations of these parameters. The bandwidth of such a source varies, but is generally in the range of 0.1–0.5%, and the photon energy instability can occasionally exceed this bandwidth. When a monochromator is inserted in the beam to perform spectroscopic measurements, the photon energy instability adds to the X-ray flux instabilities at the sample position [47]. The most straightforward approach to solving this problem has been to measure the incident X-ray flux as accurately as possible, allowing these fluctuations to be normalised out [181,182]. The drawback to this approach is that these intensity monitors need to be linear over many orders of magnitude of photon flux, which is difficult to achieve [47]. A second approach is to acquire as much data as possible in a single measurement, using techniques such as dispersive XES [183,184], XAS [138,139,142], and HEROS [185]. Though these approaches help solve the problems, they introduce further complexities, such as measuring an accurate incident photon energy spectrum to extract the XAS of the sample from the unpredictable X-ray spectrum of the incident pulse [186,139]. The most promising approach to reducing the instability of the X-FEL beam at the sample position is to seed the free electron laser, preferentially selecting a portion of the photon spectrum to initiate the lasing process [187]. The result is a significant improvement in the spectral stability of the X-FEL beam, at a cost of a factor of approximately 5–10 reduction in photon flux [188]. Though the seeded X-ray spectrum is not properly monochromatic, as it has a tail that extends a few eV to lower photon energies, it greatly enhances the pulse-to-pulse energy stability of the photon beam through a monochromator. It should be emphasised here that X-FEL facilities are under continuous improvement, and the operational characteristics vary from facility to facility. The most laser-like X-FEL currently in operation is the FERMI@Elettra facility in Trieste, which is seeded and generates VUV laser light up to 100 eV [189,174].

Perhaps the most fundamental distinction between storage rings and X-ray free electron lasers is that storage rings serve many users simultaneously while X-FELs are dedicated to a single

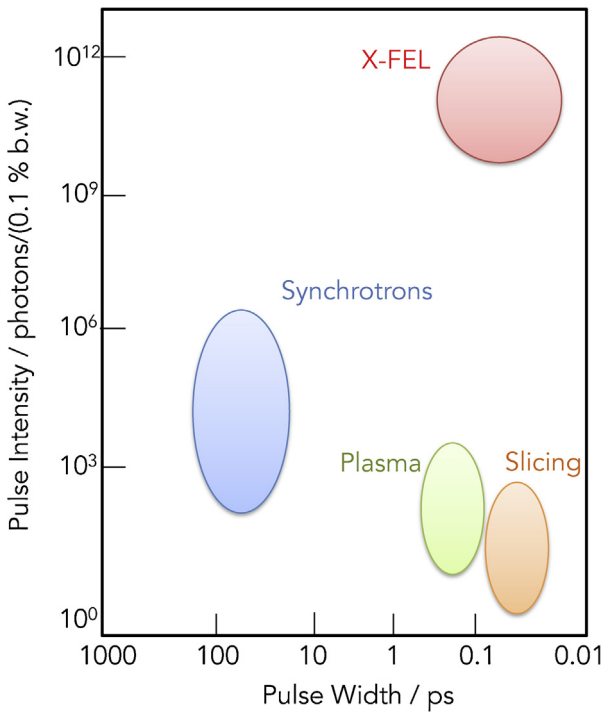

Fig. 8. A schematic showing the pulse intensities and temporal resolution of present and future sources of subnanosecond-pulsed X-rays.

experiment at a time. The advantage to this approach is unprecedented cooperation between the facility and the experiment. The experiment now has fine-grained control over all the machine parameters, allowing the users to tune the X-FEL to generate precisely the X-ray beam necessary for the experiment. The obvious disadvantage to single-user operation of an X-FEL is an enormous reduction in available measurement time at these facilities, but this is compensated by the significantly reduced data acquisition time, resulting from the high brilliance of the source. The approach taken by the LCLS facility to have simultaneous user operation is a beam sharing approach where a diamond crystal is used to diffract a narrow X-ray bandwidth beam for one experimental station while the second station uses the broad bandwidth beam transmitted through the crystal [190]. The more expensive approach taken by the European X-FEL facility (Hamburg) is to have several undulator sections operating simultaneously, allowing the facility to serve multiple users from a single electron source.

In conclusion, although these 4th-generation light sources are in their infancy, it is clear that their effect on the field of time-resolved X-ray science, which is already felt in coordination chemistry and biochemistry, will be profound and far-reaching. This is most starkly demonstrated in Fig. 8 showing the comparative peak brilliance and temporal resolution of the main X-ray sources discussed above. In this sense X-FELs are unparalleled.

4. Background of time-resolved X-ray spectroscopies

The first time-resolved XAS measurement was performed by Mills and co-workers at the CHESS storage ring. They investigated the recombination of carbon monoxide (CO) to myoglobin (Mb) after its photodissociation using a green nanosecond laser pulse [191]. The sample was probed at the iron K-edge (7.12 keV) using X-ray pulses 160 ps long, operating at a repetition rate of 390 kHz (2.56 μs between X-ray pulses). By clever binning of the total X-ray fluorescence signals they could monitor the photoexcited signal around the absorption edge over the full range of the sample

relaxation (a few μs to >10 ms) and recovery of carboxy-myoglobin. Importantly, as the authors pointed out, the data collection time and resulting signal-to-noise was controlled not by the sample or the X-ray flux, but by the laser repetition rate [192].

It took another 15 years, before time-resolved XAS experiments were implemented again. This time, at higher temporal resolution (sub-ns) and using more sophisticated laser sources (e.g. amplified Ti:Sa femtosecond lasers) able to produce pulse energies in the mJ range at kHz repetition rates. In addition, these measurements took advantage of fast X-ray detectors in transmission and fluorescence to resolve the X-ray pulse structure from the storage ring, allowing the photons from a single X-ray probe pulse to be selected electronically [143,24,193]. In this approach, data acquisition is based on the measurement of transient absorption spectra, i.e. the difference between the absorption of the excited sample minus that of the unexcited sample. The XAS signal at a specific X-ray energy and pump-probe time delay is recorded at twice the laser repetition rate, alternating between the signal from the excited sample (pumped) and that from the unexcited sample (unpumped). The laser ran at 1 kHz repetition rate and consequently the X-ray signal was recorded at 2 kHz. The 1 kHz repetition rate is determined by the excitation laser, which is a regeneratively amplified Titanium-sapphire (Ti:Sa) laser. These lasers were required to generate sufficient sample excitation in a sample volume larger than that probed by the X-rays.

These schemes allowed time-resolved measurements during normal user operation and required no specialised hardware, such as a fast X-ray mechanical chopper [194]. The experimental measurements include results on the dynamics of photoinduced structural changes in Ru and Fe polypyridine complexes [28,25,23,26], in Ni-porphyrins [195] and in Cu-diimine complexes [19,18]. However the general conclusion to be drawn from these measurements is that they require significant acquisition times (typically tens of hours), to ensure meaningful signal-to-noise ratios (S/N). In addition, the necessary sample concentrations were generally high (tens to hundreds of mMol), which excluded biological systems, that can be dissolved to at most a few mMol. In order to overcome these limitations, a number of developments were undertaken, which we present in the following sections.

5. Recent experimental developments

5.1. The high repetition rate scheme for picosecond XAS

As previously described, one of the limitations to performing time-resolved laser pump/X-ray absorption probe measurements at a storage ring has been the enormous mismatch between the repetition rate of the femtosecond amplified pump laser (1 kHz) and the storage ring (typically MHz), which has limited the data acquisition rate of the experiments. To overcome this, we implemented a scheme based on high repetition rate pump lasers allowing over an order of magnitude improvements in the achievable S/N in time-resolved XAS measurements [196]. Similar developments followed at other 3rd-generation light sources [197–199]. Importantly, besides the reduced acquisition times for XAS, these new schemes open perspectives for picosecond second-order core-level spectroscopies such as X-ray emission spectroscopy (XES), and resonant inelastic X-ray scattering (RIXS), which have low cross sections.

The setup at the SLS (Villigen) uses a high-repetition rate, high average power Nd:YVO_4 laser running at 520 kHz, i.e. half the repetition rate of the SLS (1.04 MHz). This represents the most efficient use of all the available isolated hybrid pulses, but the laser repetition rate can also be decreased if required due to sample relaxation times (>1 μs) or if higher laser pulse energies are desired. Using this setup, we demonstrated [196] an increase of the signal-to-noise ration (S/N) per scan by a factor of ~25, resulting in greatly reduced data acquisition times and the ability to measure dilute samples in the mMol range. In addition, the laser delivers 10 ps pulses at wavelengths of 1064 nm, 532 nm, 355 nm or 266 nm, rather than at 400 nm, as delivered by 1 kHz amplified femtosecond lasers. This is especially pertinent for chemical and biological systems that tend to have strong absorption bands in the green.

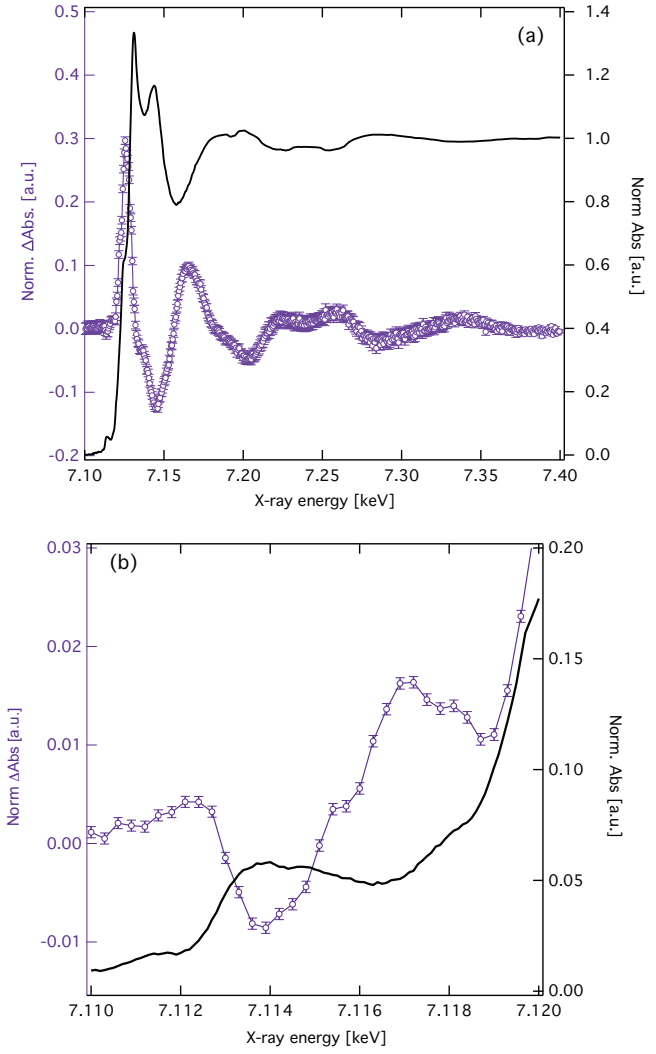

Fig. 9. Time-resolved XAS of $[Fe(bpy)_3]^{2+}$ in aqueous solution measured at the Swiss Light Source using high-repetition rate pump-probe techniques. (a) ground-state (low-spin) XAS measurement (black line) and transient XAS signal (laser on XAS – laser off XAS) measured 50 ps after excitation (purple markers). (b) zoom of the pre-edge region showing the ground-state (black line) and transient XAS (purple markers) signals.
From Ref. [196].

Fig. 9 shows the time-resolved XAS of $[Fe(bpy)_3]^{2+}$ (iron(II) trisbipyridine) in aqueous solution recorded at the Fe K-edge (7.1 keV) using the high-repetition rate pump-probe scheme. The effect of the increased S/N is observed in the improved quality of the usually weak EXAFS modulations, which is very useful for a precise structural analysis of the excited state. It also becomes possible to resolve the changes in the pre-edge transitions, which are weak because they are dipole forbidden [200], and could not be observed using the 1 kHz scheme [26]. This yields deeper insight into the electronic structure changes that are caused by the optical excitation. Our present set-up has since been used to study heme proteins in physiological solutions [196], excited state relaxation of iron, ruthenium, rhenium, and copper complexes [196,201–203] and metal

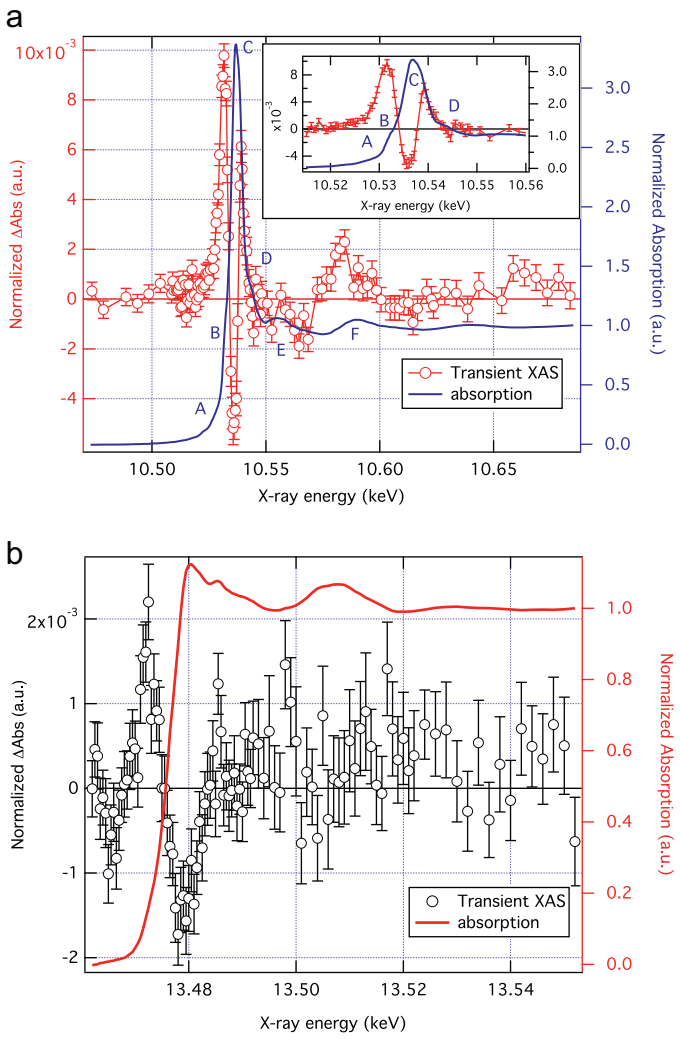

Fig. 10. Left: Normalised Re L_3-edge transient XAS signal of a 30 mM solution of $[ReBr(CO)_3(bpy)]$ in N,N-dimethylformamide (red markers) measured 630 ps after excitation with 355 nm The ground-state XAS is also shown for comparison (blue line) with features labelled A–F. Inset: zoom into the near-edge region to show the details of the transient XAS. Right: The corresponding normalised Br K-edge transient XAS signal measured on the same sample under the identical conditions. The ground-state XAS is also shown for comparison (red line).
Figures reproduced from Ref. [201].

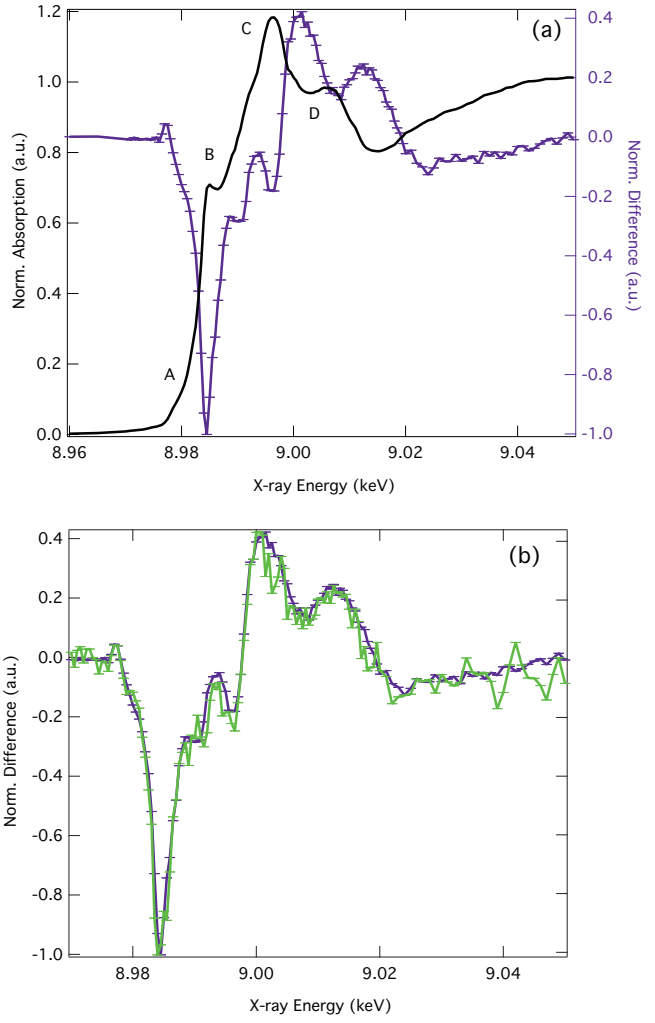

Fig. 11. (a) Static (black) and 50 ps transient Cu K-edge XANES spectra of $[Cu(dmp)_2]^+$ in acetonitrile (purple). Prominent features in the ground-state XAS are labelled A–D. (b) 50 ps transient Cu K-edge XANES spectra of $[Cu(dmp)_2]^+$ in acetonitrile (purple) and dichloromethane (green) [203]. In all cases the transient spectra have been normalised to the largest difference.

oxide nanoparticles [204]. Similar schemes at other storage rings have been used to investigate a nickel–porphyrin complex (NiTMP, Ni(II)-tetramesitylporphyrin) dissolved in toluene [197], previously studied by Chen and co-workers [195,20], and the melting of a Ge single crystal [198]. The latter demonstrates that high-repetition rate XAS techniques may also be applied to solid samples, though care must be taken to minimise sample damage.

The benefits of our high-repetition rate pump-probe set-up are highlighted in two examples shown in Figs. 10 and 11. Fig. 10a and b shows the steady-state and picosecond time-resolved spectra of $[ReBr(CO)_3(bpy)]$ at the Re L_3-edge and Br K-edge, respectively [201]. Upon excitation into the lowest CT state, the system relaxes to the triplet state faster [205] than the temporal resolution of the experiment (>50 ps) and therefore we probe the relaxed triplet state. Our transient spectra, at both the Re L_3- and Br K-edge, exhibit new pre-edge absorption peaks at 10.531 and 13.473 keV, which are attributed to the Re $2p_{3/2} \rightarrow 5d$ and the Br $1s \rightarrow 4p$ transitions, respectively, accompanied by a blue shift of the edge. These observations arise from the creation of a hole in the highest occupied molecular orbital, which has a mixed character between Re and Br [206]. Consequently, photoexcitation of this complex causes a charge transfer from the Re-Br moiety to the bpy ligand, and the long lived triplet state formed is best described as a metal/ligand-to-ligand charge-transfer (MLLCT) state.

Fig. 11 shows the static and picosecond X-ray absorption study at the Cu K-edge of $[Cu(dmp)_2]^+$ (dmp = 2,9-dimethyl-1,10-phenanthroline) dissolved in acetonitrile and dichloromethane [203]. Previous studies have reported that the phosphorescence lifetime is significantly shortened in electron donating solvents [207] and concluded that this quenching is due to complexation of a solvent molecule that most likely occurs at the metal centre. However, our transient spectra are remarkably similar for both solvents (Fig. 11b), and the spectral changes can be rationalised using the optimised excited (triplet MLCT) state – the optimised ground state structure of the complex. Contrary to previous claims [208,209], the excited-state XAS spectra do not show evidence of exciplex formation at the metal centre that was invoked to explain the luminescence quenching. This is confirmed by MD simulations, which indicate only a weak interaction between the Cu and the solvent, as shown by the distance between the two, which is ~3.5–4 Å. The strength of this interaction is comparable to a weak hydrogen bond and therefore, it undergoes rapid exchanges with the bulk solvent [203]. We concluded that instead of exciplex formation, the

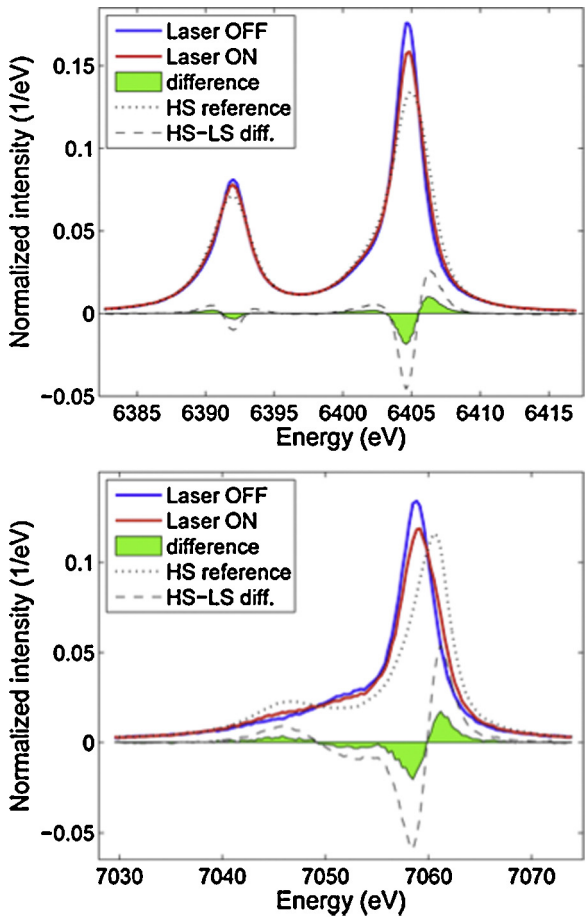

Fig. 12. Kα (top) and Kβ (bottom) spectra of $[Fe(bpy)_3]^{2+}$ with $\Delta t = 100$ ps for the laser-on data. The change from the low-spin (LS) state upon laser excitation is evident, and by direct comparison with high-spin/low-spin reference spectra, accurate determination of the high-spin (HS) fraction can be determined from the transient XES. Close to 40% HS excitation was achieved in these experiments.
The figure has been reproduced from Ref. [199].

lifetimes and solvent-dependent quenching of $[Cu(dmp)_2]^+$ can be rationalised in terms of the energy gap between the ground and ^{3}MLCT states, and the weak transient solvent interactions, already present in the ground state.

5.2. Picosecond second-order X-ray spectroscopies

The ability to exploit close to all of the photon pulses from a storage ring offers the possibility to implement photon-greedy X-ray spectroscopies in the picosecond domain. Indeed, second-order approaches such as XES or RIXS, which detect the outgoing fluorescence, are challenging due to the low count of emitted photons. However, they are powerful tools for simultaneously probing the occupied and unoccupied density of states and the spin of the emitting atom.

The photon flux associated with 3rd generation light sources has led to significant interest in these techniques. The first demonstration of picosecond XES was achieved by Vanko et al. [210] using the Fe K$\alpha_{1,2}$ (2p→1s) emission to probe the spin cross-over in photoexcited $[Fe(bpy)_3]^{2+}$. This experiment was carried out using a 1 kHz pump laser and the acquisition times were long. It was recently repeated (see Fig. 12) probing both the Kα and Kβ emissions using a high repetition rate setup [199], highlighting the power of the high repetition rate scheme as well as sensitivity of XES for determining the occupation of 3d orbitals, or more precisely, the number of unpaired electrons.

Towards pushing RIXS into the time-domain, Fig. 13 shows the RIXS spectrum of solid $[Fe(phen)_2(NCS)_2]$ (phen = 1,10-phenanthroline) in its low-spin (left) and thermally-excited high-spin (middle) states, with the difference between them shown on the right. The RIXS spectrum of aqueous $[Fe(terpy)_2]^{2+}$ (terpy = 2,2′:6′,2″-terpyridine) before and after laser excitation is shown below. Both plots show that while for the LS case there is a single resonance, there are three for the HS state, indicating a more complex electronic configuration following the spin crossover transition [200,212,213]. These changes translate into the ones found in resonances that are less distinguishable in traditional time-resolved XAS due to the lifetime broadening and the overlap of the peaks on the X-ray absorption axis (see Fig. 9).

5.3. Femtosecond XAS at storage rings

As already mentioned, the physics of storage rings limits the X-ray pulse duration to tens of ps. In order to reach fs timescales, the laser-electron slicing scheme was implemented at 3rd generation storage rings [38–41]. Briefly, a high pulse energy femtosecond laser is overlapped in time and space with the electron bunch in the storage ring and co-propagated through a specially designed wiggler (modulator). The wiggler optimises the interaction between the electrons and the laser pulse, resulting in a modulation of the electron energies in a femtosecond slice. The electrons then proceed through a dispersive region of the ring, separating them spatially as a function of energy, and are sent through an insertion device (undulator), generating fs X-ray pulses. The latter can then be spatially isolated using a combination of X-ray optics and slits. The result is a femtosecond X-ray pulse at the end of the beamline, with all the advantages inherent to the beamline (fixed-exit, double-crystal monochromator, microfocussing KB mirrors, experimental setup, etc.). The stability requirements for XAS is fulfilled with the slicing source, however due to the fact that the electrons modulated in energy represent only a 100 fs slice out of a typically 100 ps electron bunch, the X-ray photon flux generated by these sources at a given energy is very low, which has made XAS experiments difficult. For ultrafast X-ray diffraction measurements [214–222], these sources have been used with success since one can use a broader bandwidth incident spectrum, at the expense of energy resolution, without any measurement degradation.

Despite the more stringent requirements for femtosecond hard XAS studies due to the need of energy resolution (~2 eV), it has still been possible to carry out successful femtosecond XAS experiments. The first example in solution was the study of ultrafast spin-crossover dynamics of $[Fe(bpy)_3]^{2+}$ in aqueous solution probed at the Fe K-edge after photoexcitation. This measurement showed that the population of the high-spin quintet state from the initially populated singlet metal-to-ligand-charge-transfer (MLCT) state is remarkably fast (<150 fs), resolving a long-standing debate about the population mechanism of the quintet state [44,223]. Later Pham et al. [45] used fs XAS to probe the transition from hydrophilic to hydrophobic solvation following electron abstraction from aqueous iodide, at the I L_1 (see Fig. 14) and L_3 edges. This study showed the existence of a short lived $I^0\cdots(H_2O)$ intermediate species with a single water molecule forming a 3 electron bond with iodine [224,225].

The Advanced Light Source (ALS, Berkeley, USA) and the BESSY II (Berlin) storage rings were the first to implement the laser-electron slicing in the soft X-ray range. The femtosecond XANES of the insulator-to-metal phase transition in VO_2 was investigated [226]. Measurements around the O K-edge (530 eV) and V L_3-edge (516 eV) made it possible to extract dynamical information on the electronic band states near the Fermi level during the phase transition. The slicing source at the ALS was also used to

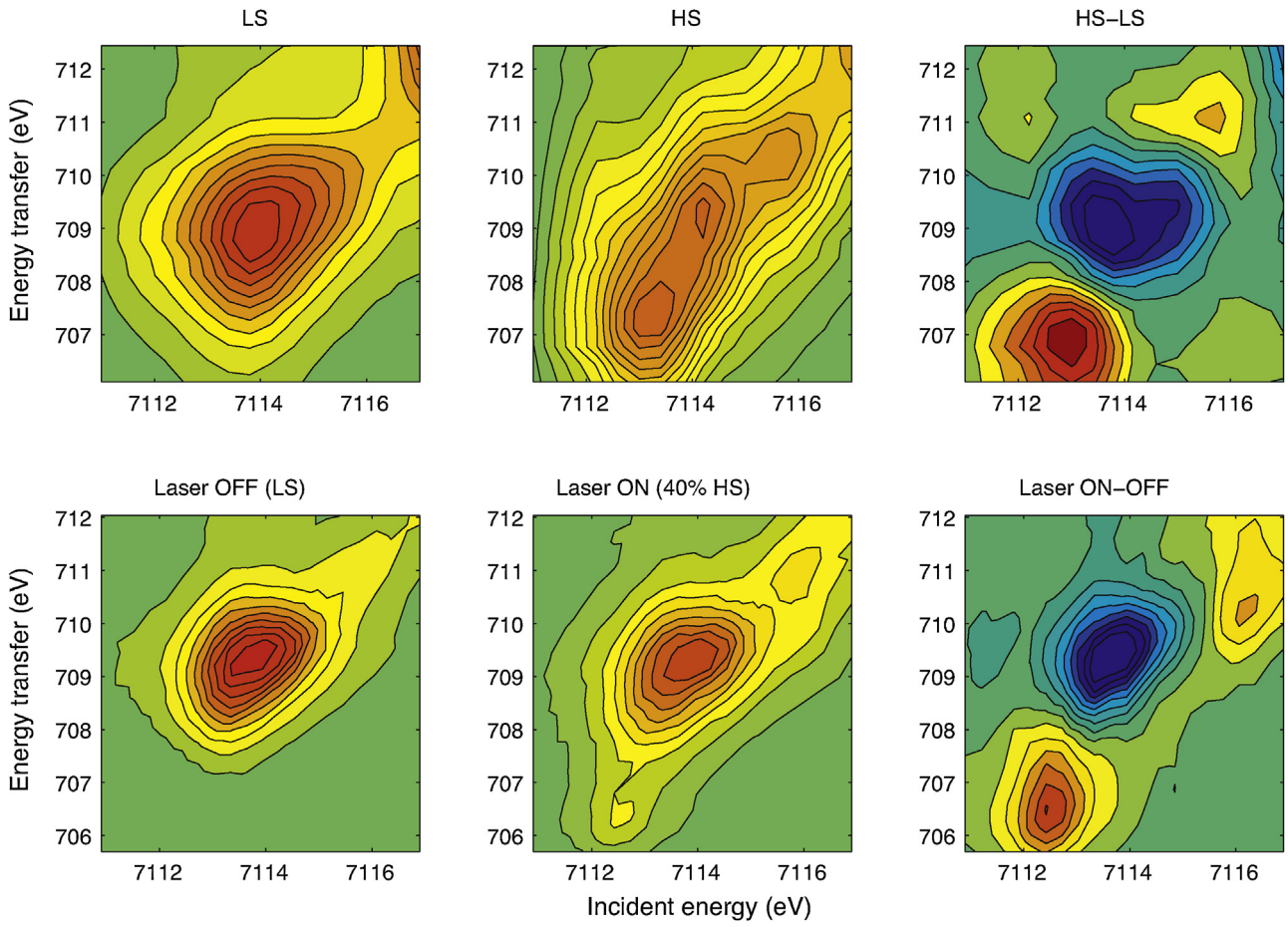

Fig. 13. Top: $1s2p_{3/2}$ RIXS plane of solid $[Fe(phen)_2(NCS)_2]$ in its low-spin (left) and thermally-excited high-spin state (middle), with the difference between them shown on the right. Bottom: $1s2p_{3/2}$ RIXS plane of aqueous $[Fe(terpy)_2]^{2+}$ before (left) and after laser excitation (middle), with the difference between them shown on the right. From Ref. [211].

probe the dynamics of liquid water after IR excitation of the O—H stretching vibration [227]. The measurements on the hundreds of ps timescale showed changes in the O K-edge XAS consistent with an increase of temperature and pressure in the water

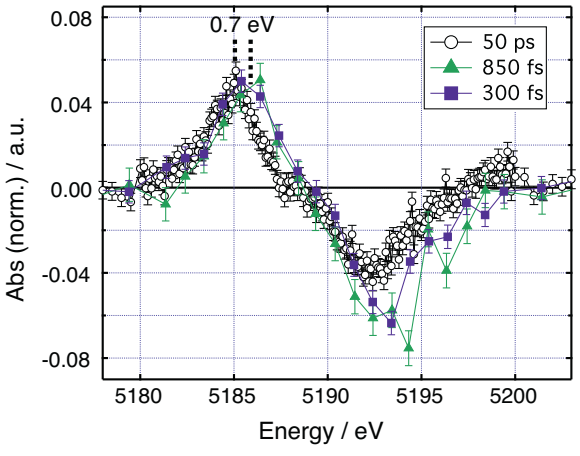

Fig. 14. Normalised transient L_1-edge spectra of photoexcited aqueous iodide at 50 ps (black markers), 300 fs (green markers), and 850 fs (purple markers) time delays after excitation. The sub-picosecond transients were multiplied by a factor of 1.75 in order to match the value of the 50 ps transient at the maximum of the positive feature. Note the 0.7 eV shift to higher energies of the early time transient compared to the late time transient.
Reproduced from Ref. [45].

[228–231]. The fs time scans showed the formation of this state with a time constant of 700 fs. This approach was then applied to a spin-crossover molecule, $[Fe(tren(py)_3)]^{2+}$ (tren(py) = tris(2-pyridylmethyliminoethyl)amine), dissolved in acetonitrile. Ps measurements at the Fe $L_{2,3}$-edges [31,232] showed clear evidence of a smaller ligand field in the high-spin state and reduced interaction between the Fe orbitals and the ligands, resulting in a large shift to lower energies of the absorption edges. Femtosecond measurements using the ALS slicing source revealed a timescale of formation of the high-spin state of 150 ± 60 fs [46].

The slicing source at BESSY II has been used primarily for resonant diffraction, XAS, and X-ray magnetic circular dichroism (XMCD) measurements around transition metal L-edge resonances (200 eV to 1 keV) of solids [233–237]. An example is the measurement [233] of photoexcitation of a 15 nm Ni thin film where the transmission XAS signal with linear polarisation showed a 130 meV shift of the Ni L_3-edge to lower energy on a timescale of 120 ± 50 fs, followed by a slower relaxation on a timescale of 640 fs. They attributed the fast signal to the electronic response to laser excitation, followed by the slower electron-lattice relaxation time. It was concluded that the majority of the time-resolved signal stems from changes in the spin angular momentum (S) and not from the orbital angular momentum (L) of the 3d electrons, i.e. spin angular momentum is transfer to the lattice on a fs time scale. These measurements showed the ability to separate the spin and orbital angular momentum components on a femtosecond timescale with elemental sensitivity, and paved the way for future measurements [236,237].

In conclusion, the low photon flux of the slicing sources is the major limitation to their widespread use, especially for measurement of dilute solutions. In addition, despite the perfect synchronisation between the pump pulse and the sliced X-ray probe, the data acquisition times caused by the low flux imply long time drifts, which tend to decrease the time-resolution. Finally, second-order spectroscopies are excluded with the slicing scheme.

5.4. Femtosecond X-ray spectroscopies at X-FELs

The flux limitations of the slicing scheme has now been overcome with the advent of X-FELs. The flux is typically 10–11 orders of magnitude higher than the slicing source, opening new perspectives for performing fs X-ray diffraction and spectroscopy experiments [166], single-shot structural experiments [238–240], and nonlinear X-ray experiments [241]. Because of the inherent instability in both the photon energy, the pulse energy, and the pulse arrival time of these sources, it has not been a straightforward task to perform time-resolved XAS measurements with them. However, since its initial operation in 2009, the LCLS has introduced a number of improvements, such as accurately measuring the timing jitter between the laser pump and X-ray probe pulses on a shot-to-shot basis [242,243] or improving the photon energy stability through hard X-ray self-seeding [188].

Recently Lemke et al. [47] demonstrated the proof of principle of pump-probe Fe K-edge XAS measurement performed at the LCLS on an aqueous solution of $[Fe(bpy)_3]^{2+}$. The results are consistent with the measurements made using the FEMTO slicing source at the SLS [44] and in the UV [244]. However, due to timing jitter the time-resolution was poorer than the latter. The recent introduction of the LCLS 'timing tool', which measures the timing jitter between the laser and the X-rays, should allow measurements with <100 fs time resolution [242]. However, this measurement also highlights the difficulty of accumulation techniques for X-FEL experiments, which is made challenging by the large intensity fluctuations and detector nonlinearities [47]. Consequently, there is great interest in single shot techniques [139]. A recent example as discussed above is the high energy resolution off-resonant spectroscopy (HEROS) combined with a wavelength-dispersive type spectrometer based on the von-Hamos geometry [88], which has recently been demonstrated at LCLS [185].

The demonstration of the feasibility of time-resolved XES at 3rd-generation light sources offers much promise for their implementation in the femtosecond regime at X-ray free electron lasers, thanks to the three orders of magnitude shorter pulse duration and ten orders of magnitude increases in the flux of the pulses. In addition, these measurements can be simultaneously carried out with time-resolved scattering on the same samples by placing a 2D detector behind the liquid jet [199], providing the opportunity to obtain both the global geometric structure and the electronic structure around the absorbing atom simultaneously. This approach has also recently been applied to study photosystem II (PSII). In an initial paper, Alonso-Mori et al. [183] obtained energy dispersive X-ray emission recorded in a shot-to-shot mode probing the electronic structure of redox-active metal sites, Mn^{2+} and $Mn_2^{3+/4+}$ of photosystem II by $K\beta_{1,3}$ XES. Later, they combined X-ray diffraction (XRD)-XES and demonstrated the power of simultaneous global geometric and electronic structure determination [184], which offers exciting new directions for time-resolved studies. Importantly these results demonstrated the power of femtosecond X-ray pulses on biological samples, as they could show that the samples were not damaged due to the ultrashort duration of the pulse contrary to in the case of previous studies at 3rd generation storage rings. Indeed, XES was used as to monitor the chemical integrity of the sample showing that the electronic structure of these metal sites at room temperature remained intact during the XRD measurement.

Even with these issues, the advantages of X-FELs are substantial and offer new opportunities for second-order spectroscopies, scattering studies [245–248], and non-linear core-level spectroscopies. One particularly promising approach is stimulated core-level emission spectroscopies, which have the potential advantage that, as in the optical domain, the stimulated process surpasses the spontaneous one, with efficiency gains of up to 7 orders of magnitude [249]. Such experiments require ultrashort, temporally coherent, synchronised two-colour X-ray sources. At present this is a restriction of the present SASE free-electron lasers which have a fluctuating spectrum and limited temporal coherence [149,159]. However, using 960 eV X-FEL pulses focused onto neon gas, Rohringer et al. [250] showed stimulated emission from the Kα fluorescence line, and the demonstrated lasing has exhibited a more reproducible spectrum and a much narrower bandwidth than the SASE X-FEL pulse. Following this, Beye et al. [251] have demonstrated stimulated X-ray emission of crystalline silicon concluding that stimulated emission can enhance the detected signal by several orders of magnitude.

At present, the only possibility to carry out core-level nonlinear spectroscopies [252–254] is at the FERMI@Elettra seeded VUV FEL [189]. FERMI@Elettra can generate coherent nearly transform-limited pulses at a repetition rate of 10 Hz at wavelengths that are integer fractions of the seed laser fundamental wavelength (~260 nm), i.e. at 65.0, 52.0, 43.3, 37.1, 32.5, 28.9, 26.0, 23.6, 21.6, 20.0 nm. Because of seeding, the machine is extremely stable in terms of intensity ($\Delta I/I < 0.1$) and delivers pulses with intensities above 200 μJ (for wavelengths >35 nm). The pulse duration is estimated to be $\tau_{FEL} \sim \tau_{seed} * n^{-1/3}$, where n is the seed harmonic number and $\tau_{seed} \sim$ 180 fs. The possibility to perform non-linear X-ray experiments at FERMI@Elettra on coordination chemistry complexes has recently been explored and offers promising prospects [255].

6. Theoretical developments

The progress of experimental techniques for core level spectroscopies, outlined above, is unravelling subtle spectral features implying that high level theoretical approaches are required to interpret them. For time-resolved experiments, the precision of the theoretical approaches is particularly pertinent as both the ground and excited state spectrum must be accurately simulated to obtain the transient spectrum. At the temporal resolution of 3rd generation storage rings these can generally be considered *quasi-static*. This is to say that the response of the system and surrounding environment occurs within the temporal width of the X-ray probe and consequently dynamical effects can often be neglected in the simulations. Therefore the transient spectrum is simulated as the optimised metastable excited state or product minus the optimised ground state. In the following sections we give a brief background to simulating core-level spectra before outlining some recent developments. We then discuss the future challenges for the theory, especially in regards to its application to ultrafast core-hole spectroscopies in which the *quasi-static* approximation may break down.

6.1. Background to simulating X-ray spectroscopies

Calculating core-hole spectra involves two principal steps. First, the ground state electronic structure of the system is calculated (see Section 6.2) and then the effect of the perturbation by the X-ray pulse is determined (see Section 6.3). For the latter the simplest approach is the single-particle picture. Here a single electron makes

a transition from a core orbital to an excited state and the transition energy corresponds to the energy difference between the orbitals occupied in the ground and excited states (this obviously neglects many-body effects). Within this approximation, the major challenge is the difficulty associated with calculating the final state wavefunction. This has traditionally been overcome using multiple scattering theory (MST), which can easily calculate unoccupied states for large excitation energies. Here, Fermi's Golden Rule (Eq. (2)) is rewritten in the form of a Green's functions [48,256–258]:

$$\mu(E) \propto -\frac{1}{\pi}\Im\sum_i |\langle i|\epsilon\cdot\mathbf{r}G(\mathbf{r},\mathrm{r}\prime;E)\epsilon\cdot\mathrm{r}\prime|i\rangle| \quad (8)$$

This has the advantage of compressing the sum of the final states and energy conversing delta function into a Green's function propagator, $G(\mathbf{r}, \mathbf{r}', E)$, which can be expressed as contributions of the absorbing atom (G^c) and the surrounding atoms (G^{sc}):

$$G(\mathbf{r},\mathrm{r}\prime;E) = G^c(\mathbf{r},\mathrm{r}\prime;E) + G^{sc}(\mathbf{r},\mathrm{r}\prime;E) \quad (9)$$

G^{sc} is then either solved as a sum over MS paths or as a matrix inversion, i.e. full MS [259]. This gives rise to a short range order theory, which is advantageous for XAS, as inelastic losses usually limit the distance probed by XAS experiment to ~6 Å around the absorbing atom.

When strong electron correlations (many-body effects) become important, as often encountered for $L_{2/3}$-edge spectra, atomic multiplet based approaches [260,49] are widely used. Atomic multiplet theory [261] solves the many-body states by taking advantage of the nature of the electron–electron interactions, which are split into spherical and non-spherical components. The former is included in the atomic Hamiltonian and forms the average energy of a particular electron configuration. The non-spherical part, in conjunction with spin–orbit coupling, acts as a perturbation and gives rise to the different terms within atomic configurations [262]. The main advantage of this approach is its computational efficiency and, for systems containing symmetry, it often achieves excellent agreement with experimental spectra. However, it does rely on a large number of semi-empirical parameters which are used to describe the effects of electron–electron repulsion, the ligand environment and covalency.

6.2. The ground-state potential

For simulating core-hole spectra there are four main approaches: i) real space multiple scattering [263–265], ii) plane waves [266–269], iii) atomic localised basis sets [270–272] and iv) atomic multiplets [273,274]. As previously mentioned, all of these calculations first require the determination of the ground state electronic structure of the system, which is then perturbed by the X-ray pulse. Here we outline some aspects of each of these frameworks, highlighting advantages and limitations.

In contrast to quantum chemistry calculations usually based upon plane waves or atomic localised basis sets, the principal advantage of MST is that it does not rely on a basis set expansion of the global wavefunction. Instead, the global solution is expanded in terms of local solutions of the Schrödinger equation at the energy of interest [275]. The separation of the propagator (Eq. (9)) into individual scattering sites imposes non-overlapping cells for the description of the ground state electronic structure and these are usually approximated as spherically averaged muffin-tin (MT) potentials. However, while this approximation is sufficient for the EXAFS region of the spectrum, it often breaks down close to the edge in the XANES region. These problems are most commonly encountered in the case of open structure systems, or when the absorbing atom is not fully coordinated meaning, in both cases, that the approximated interstitial region is large [276,277].

The generalisation of MST to full-potential was proposed in the early 1970s [278,279] and later applied to XAS by Natoli et al. [280,281]. Recently, Ankudinov et al. [282] and Hatada et al. [283,284,54] have implemented approaches for MST, beyond spherical potentials, for which the full potential is partitioned into non-overlapping cells. Although promising, at present neither have been widely applied. The most common alternative method is the finite difference method near edge structure (FDMNES) approach by Joly [285,263], which enforces no shape restrictions on the potential. Here the wavefunction is solved on a discretised three-dimensional grid. Despite significant advantages compared to calculations within the MT potential, the major limitation is that these calculations are computationally expensive and in the absence of symmetry, are difficult to apply to clusters of more than 30 atoms [286].

Methods based on atomic localised basis sets are well developed and provide highly accurate treatments of the electronic structure. These approaches are widely used to simulate bound–bound transitions in core-hole spectra (see Sections 6.3.1 and 6.3.2), however such basis sets do not generally have the flexibility to be applied to the higher energy states, i.e. the continuum [287] and in this regime, plane wave basis sets are more suitable [266–269,288,289]. This basis set is most widely used for periodic systems, and attractively its quality is controlled by a single energy-cutoff value. However, pseudopotentials have to be used for the core levels and the projector augmented wave method [290] is implemented to calculate the transition strengths in the absence of the core-electrons. Although neglecting the core-electrons reduces the computational cost making it possible to tackle larger systems, it is important to stress that it is not easy to transfer pseudopotentials between different computational packages and that they must be tested extensively in different chemical environments to ensure accurate calculations. To avoid problems associated with neglecting the core electron, an alternative is the Gaussian augmented with plane waves (GAPW) approach [291–294]. Here, a Gaussian basis set is augmented with plane waves in order to treat the diffuse region of the density. The advantage in this case is that maintaining a Gaussian atom centre basis means that this approach can be applied without the need for pseudopotentials.

6.3. Excited states and many-body effects

The simplest approach for addressing core-excitations is, as previously mentioned, the single-particle picture. Here only a single electron makes a transition from a core orbital to an excited state, and therefore this ignores many-body and charge transfer effects which can be crucial for an accurate description of the spectrum. Recently, there has been significant development in approaches aimed at addressing the limitations of both single-particle and multiplet approaches, which we will now describe.

6.3.1. Time-dependent density functional theory

Among the most recent approaches for simulating core-hole spectra is time-dependent density functional theory (TDDFT). This provides the framework to calculate excited-state energies and transition probabilities, based upon the result of a DFT calculation [295–297], and owing to its favourable balance between accuracy and computational cost has become widely used. The Linear-response TDDFT (LR-TDDFT), which we will from now on simply refer to as TDDFT, may be expressed in the form of a Dyson-like equation written [298]:

$$\chi = \chi_0 + \chi_0(v + f_{xc})\chi, \quad (10)$$

where χ_0 is the polarisability of the non-interacting system, v is the Coulomb potential and f_{xc} is the exchange-correlation (x–c) functional, which within the adiabatic approximation is defined as

$\delta^2 E_{xc}[\rho]/\delta\rho(\mathbf{r})\delta\rho(\mathbf{r}')$ [297]. The description of f_{xc} is responsible for corrections to the independent-particle approach and as its exact form is unknown, the accuracy of these calculations is determined by the approximations made within this term.

Both Ankudinov et al. [299] and Bunau and Joly [300] have implemented approaches, based on the local density approximation of the *x–c* functional, within the FEFF and FDMNES codes, respectively and used it to study the $L_{2/3}$-edges of some transition metals compounds. Their results show improvements in the L_2:L_3 branching ratio compared to the independent-electron approximation, and its effectiveness especially regarding the less localised 4d and 5d electrons. However these approaches become insufficient when the core hole multiplet effect becomes large, mainly in the case of open 3d-shell systems.

The most common application of TDDFT is within the quantum chemistry community. Here, because the pre-edge region of XAS predominately involves probing transitions between bound states below the ionisation potential, they can often be simulated using atom centred gaussian basis sets as implemented in a number of quantum chemistry codes [270–272,301,302]. Similar methods based on simple ground state DFT calculations have been applied to interpret XES transitions, which are also between bound states [72–79]. Besides a couple of notable exceptions [303,304] approaches are usually based upon Casida's formalism [305,297] (an expansion in electron-hole pairs) written:

$$\begin{pmatrix} \mathbf{A} & \mathbf{B} \\ \mathbf{B} & \mathbf{A} \end{pmatrix} \begin{pmatrix} \mathbf{X} \\ \mathbf{Y} \end{pmatrix} = \omega \begin{pmatrix} \mathbf{1} & \mathbf{0} \\ \mathbf{0} & -\mathbf{1} \end{pmatrix} \begin{pmatrix} \mathbf{X} \\ \mathbf{Y} \end{pmatrix}, \tag{11}$$

The excitation energies are then computed using this non-standard eigenvalue equation, where ω are the transition frequencies and **X** and **Y** represent excitation and de-excitation operators, respectively. The matrix elements $A_{ia,jb}$ and $B_{ia,jb}$ are written:

$$A_{ia,jb} = (\epsilon_a - \epsilon_i)\delta_{ai,jb} + (ia|jb) + (ia|f_{xc}|jb), \tag{12a}$$

$$B_{ia,jb} = (ia|jb) + (ia|f_{xc}|jb). \tag{12b}$$

For a one-electron excitation described as the transitions from an initial orbital *i* and final orbital, *a*, the first term of Eq. (12a) is the energy difference between the two Kohn-Sham orbitals, the second represents the Coulomb interaction of the electrons, and the final is the exchange-correlation energy. Eq. (11) is often solved by neglecting the **B** matrix. This is called the Tamm-Dancoff approximation (TDA) [306] and means that the de-excitation components of the excited state energies are neglected.

The extension of this to core-excitations is achieved by projecting onto a manifold of single core-to-valence excitations [307] and therefore only excitations from, for example, the 1s orbital are calculated. Besides the restricted excitation space, which introduces a negligible error [308,309], the formulation remains the same as for valence excitations. Core-hole TDDFT has now been widely used for simulating static spectra [203,200,310–317] and evidence of its accuracy is highlighted in simulations of transient (excited–unexcited) signals [203,200], such as the picosecond XAS study at the Cu K-edge of a Cu-phenanthroline complex, $[Cu(dmp)_2]^+$ [203]. The ground state spectrum of this complex (Fig. 15a) consists of two principal transitions of 1s→MLCT (A) and 1s → 4p (B), respectively. Fig. 15b shows the transient signal (i.e. the ^{3}MLCT state – ground state) compared to the experimental transient 50 ps after photo-excitation. This is characterised by a weak positive feature (A′) and negative signals corresponding to the A and B features in the ground state. The positive feature is due to the 3d hole created by photo-excitation, while the simulations demonstrate that the loss of features A and B are associated with a blue shift of features present in the ground state due to the photoinduced oxidation state change of the metal centre.

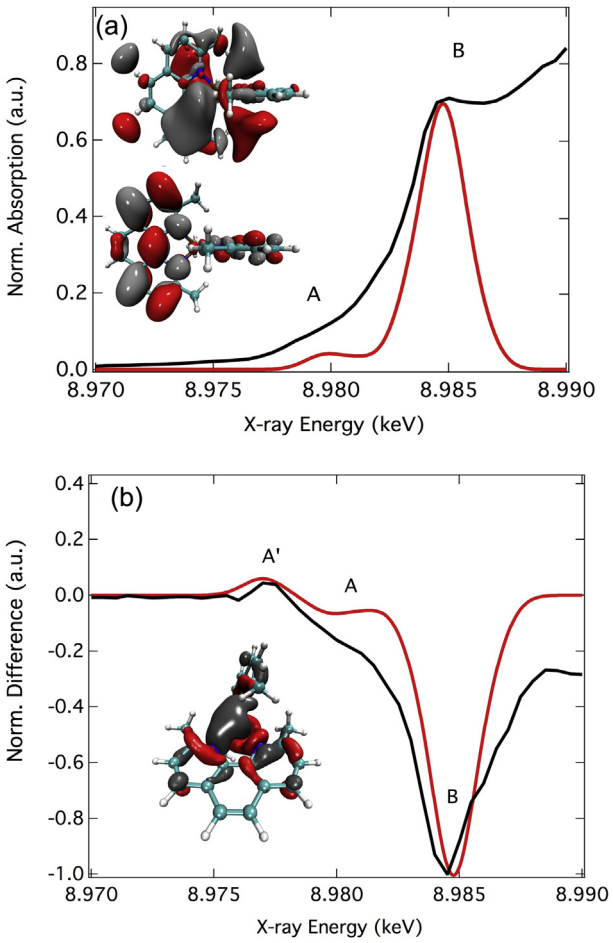

Fig. 15. (a) The pre-edge region of the spectrum and the oscillator strengths calculated using TDDFT with a 1.89 eV Lorentzian broadening. Inset is the molecular orbitals for the transition with the largest oscillator strengths for the two features. (b) The simulated pre-edge transient spectrum (red, ^{3}MLCT – ground-state) using TDDFT in comparison to the experimental transient (black). Inset is the molecular orbital for the transition with the largest oscillator strengths for the A′.
Reproduced from Ref. [203].

Despite its ability to simulate both ground and excited state spectra, it is important to recognise that TDDFT is not a *black-box* method and crucial to all simulations is the form of the *x–c* functional (f_{xc}). The most widely documented limitation of TDDFT is for charge transfer (CT) excitations, which are underestimated, as the non-local spatial character of these excitations is not captured within the inherent local nature of the *x–c* functionals [318]. Core excitations, in contrast to valence excitations, are highly localised, however CT problems can still affect the spectra as recently demonstrated using simulations of the Mn K-edge pre-edge spectra of $[Mn(II)(terpy)Cl_2]$ [319] and the Fe K-edge pre-edge of $[Fe(bpy)_3]^{2+}$ [200]. In such cases hybrid functionals, which incorporate a fraction of Hartree-Fock exchange and therefore non-locality into the *x–c* functional, are important. Besides CT, the absolute excitations energies from core levels are underestimated within TDDFT [320] and consequently the calculated spectrum must be shifted post-calculation. This error originates from the incorrect asymptotic behaviour of the potential arising from the self interaction error (SIE) [297] and while the relative spacing between the transitions remains most important, it is desirable to quantify and/or reduce this error. DeBeer-George et al. [321] have demonstrated, using a range of model systems, that this error can be calibrated, within the limit of the same calculation protocol. Alternatively, recent work has shown that the so-called range separated (RS) functionals can

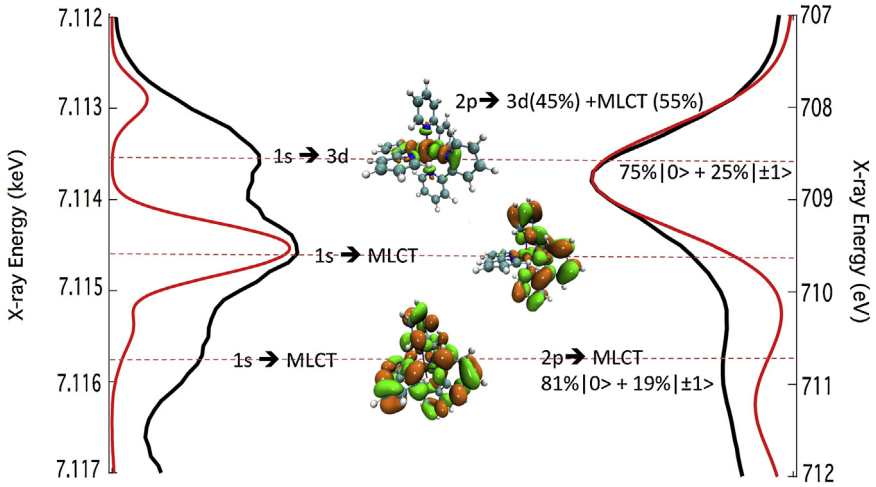

Fig. 16. A comparison of the features appearing in the pre-edge region of the Fe K-edge XAS (left) with the $L_{2/3}$ XAS edges (right) of $[Fe(bpy)_3]^{2+}$. The important molecular orbital is shown alongside the corresponding transitions. The principal states and, in the case of the $L_{2/3}$-edges, spin contributions are summarised with the respective transitions.

Reproduced from Ref. [200].

significantly reduce this problem. Here, the amount of Hartree-Fock exchange incorporated into the electron repulsion operator is partitioned into short and long-range (SR/LR) components. For core-hole excitations, a significant improvement can be obtained by including a large fraction of Hartree-Fock exchange at short-range which reduces the SIE for the localised core orbital [322,323,309,200].

6.3.2. Post Hartree-Fock methods

Density functional based approaches are sufficient to simulate pre-edge spectra, however the one-particle/one-hole (linear response) approach does not incorporate the necessary physics to account for multiplet effects arising from electron–electron correlations. In addition, the standard formulation of TDDFT, within the adiabatic approximation does not include spin-flip excitations [297], and therefore is usually unsuitable for simulating the $L_{2/3}$-edges. Consequently, there has been significant development in high level *ab initio* methods for core excitations. Towards accounting for these correlation effects, approaches based coupled cluster theory [324,51,325,326] and Algebraic Diagrammatic Construction (ADC) have been implemented [327–331]. Alternatively, Configuration interaction (CI) methods have also been implemented [332,53,333,334]. Here, the wavefunction is expressed as a linear combination of Slater determinants (or configurations):

$$\Psi = A_0|\Phi_0\rangle + A_i^a|\Phi_i^a\rangle + A_{ij}^{ab}|\Phi_{ij}^{ab}\rangle + \cdots \quad (13)$$

where the labels i, j represent occupied spin–orbitals in the reference (Φ_0), usually Hartree-Fock determinant and a, b represent unoccupied ones. The aim of including multi-configurations, generated by excitations from the reference wavefunction (e.g. Φ_i^a and Φ_{ij}^{ab}), is to increase the flexibility of the wavefunction. Full configuration interaction (FCI), where the excitations are expanded up to all orders, yields the exact wavefunction within the basis set limit, however it is not realistic as the number of configurations grows factorially with the number of electrons in the system. Therefore a truncation of the sum is usually performed, e.g. up to double excitations (CISD) as shown in Eq. (13). Recently, Neese and co-workers [53,333] have proposed a combined DFT and restricted open-shell configuration interaction method (DFT/ROCIS). Their approach expands the reference wavefunction into five excitation classes [53] aimed at describing important correlation effects for a large range of systems and includes spin flip excitations through quasi-degenerate perturbation theory [335]. Importantly for transition metal complexes, a Hartree-Fock reference represents a poor starting point due to the neglect of electron correlation (mean-field approximation) [335]. To overcome this, they incorporated restricted open-shell Kohn-Sham orbitals into the CI matrix, for which the parameters of the mixing have been obtained from a fit to a test set of molecules, similar to the approach of Grimme et al. [336,337]. While introducing an empirical aspect into the approach, this enables calculations on large systems and its effectiveness has recently been demonstrated for the L-edge of Vanadium complexes and lattices [338,339] and the static and picosecond $L_{2/3}$-edge of $[Fe(bpy)_3]^{2+}$ [200]. The $L_{2/3}$-edge ground state spectrum of the latter, simulated using the DFT/ROCIS method, is presented in Fig. 16. The agreement with experiment is good and using the high-resolution Fe K-edge pre-edge spectrum of $[Fe(bpy)_3]^{2+}$ (Fig. 16 left) it was possible to provide an interpretation of the features arising in both spectra and their relationship with respect to selection rules [200].

For complex systems, which include strong spin coupling, open-shell states and/or degeneracies, the aforementioned methods can break-down and a higher level of theory is required. One such class of methods is the Multi-Configurational Self-Consistent Field (MCSCF) method [340], among which the most commonly adopted approaches are Complete Active Space Self Consistent Field (CASSCF) and Restricted Active Space Self Consistent Field (RASSCF). Here the spin orbitals are split into inactive and active subspaces, and the wavefunction is generated by occupying the active orbitals in all ways, consistent with the desired overall spin and space symmetry [341], i.e. full CI within an active orbital subspace (see Fig. 17a). In choosing only the most important orbitals for the active space, this method allows a complete set of the important determinants to be described, while the reduced configuration space limits the computational expense. Using such an approach, Josefsson et al. [52] presented an extension of RASSCF and RASPT2 methods to core excitations. This has since been more widely applied [342,98,343]. RASPT2 is a second order perturburative correction that incorporates dynamic correlation [344] not accounted for in RASSCF, which is often important for transition metals. As shown in Fig. 17, this approach has been successfully applied to calculate the $L_{2/3}$-edge and RIXS spectra of aqueous Ni^{2+}. Fig. 17a shows a schematic of the molecular orbitals and highlights the orbitals incorporated into the active space to correctly describe the spectrum, which involve Ni 2p and Ni 3d, partitioned into two subspaces. The $L_{2/3}$-edge compared to experiment is shown

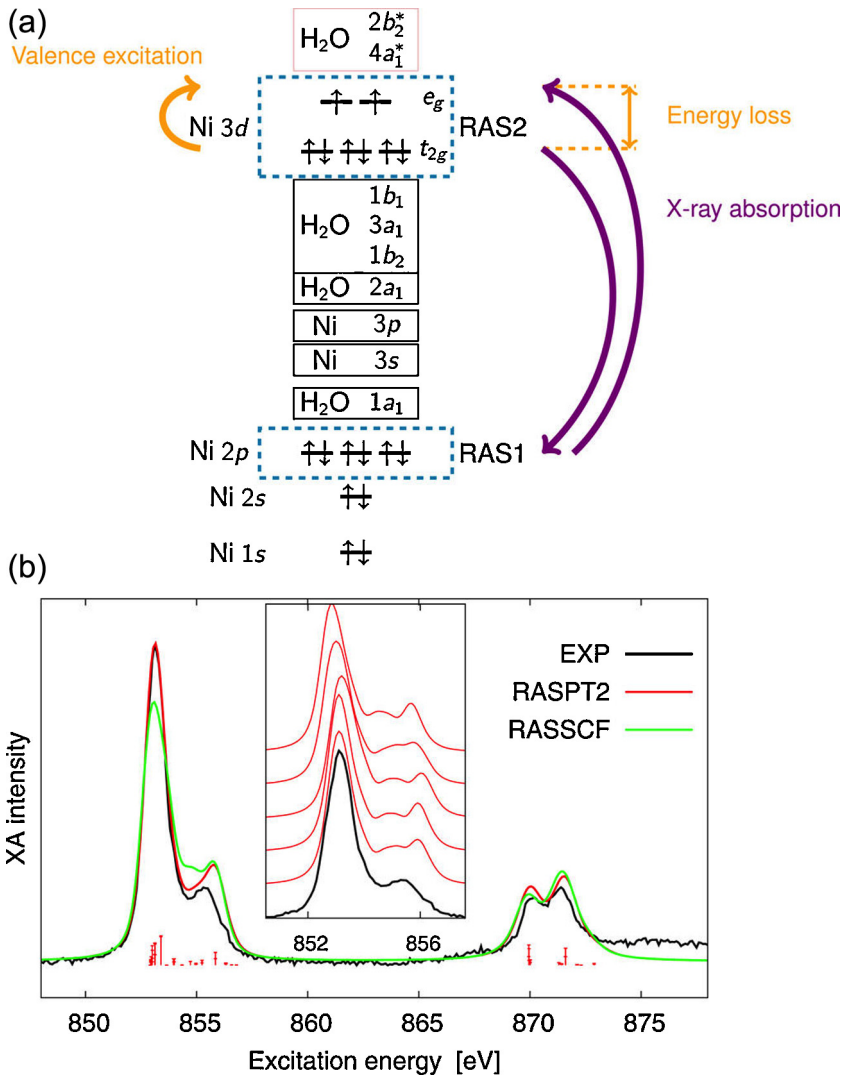

Fig. 17. (a) Schematic of the active space of the $L_{2/3}$-edge of aqueous $NiCl_2$. The Ni 2p and Ni 3d are partitioned into two subspaces. RAS1 contains the Ni 2p orbitals with at most one hole, whereas RAS2 allows all possible electron permutations in the Ni 3d orbitals. Ligand-to-metal charge-transfer (LMCT) excitations can be accounted for by introducing ligand orbitals in RAS1 or RAS2. By introducing ligand orbitals in a third subspace RAS3 containing at most one electron, we can also model metal-to-ligand charge-transfer (MLCT) excitation. (b) Comparison between the experimental XAS of aqueous $NiCl_2$ and XAS calculated for $Ni^{2+}(H_2O)_6$, with the RASSCF and RASPT2 methods. Reproduced from Ref. [52].

in Fig. 17b, and in both cases (RASSCF and RASPT2) the agreement with the experimental spectrum is good, however the effect of dynamic correlation on the Ni 3d orbitals is highlighted in the relative magnitudes of the peak intensities.

In summary, the RASSCF and RASPT2 approaches to core-hole excitations highlights that calculating such spectra from first principles using high-level quantum chemistry approaches is now possible. However, it should be stressed that the successful application of these approaches requires a careful choice of the active space, which is not always straightforward. In addition, the computational expense scales exponentially with the size of the active space and often represents the limiting factor. This also excludes them for solid state systems. Alternatively the DFT/ROCIS adopts a somewhat more pragmatic approach by accounting for dynamic correlation in a semi-empirical manner. Although no longer first principles, this approach incorporates the correct physics to tackle spin–orbit coupling and multiplet effects for a wide range of systems and particularly in the case of larger systems.

Finally, important in the context of recent experimental developments, is that the <100 fs temporal resolution, as offered by the X-FELs, implies that the *quasi-static* approximation will break down and therefore an explicit description of the excited state dynamics of the system will be necessary. In this regard an accurate description of the excited state wavefunction must be used as a reference determinant for simulating the experimental observables. This is not possible within standard implementations of TDDFT (unless the excited state is the lowest state of a particle spin multiplicity), as the excited state is calculated from the response of the ground state density to a perturbation (by the X-ray field). However, such calculations are feasible within the aforementioned post-Hartree Fock approaches. Here, the excited state can be addressed by either forcing population of an excited orbital during the self-consistent field procedure, which might suffice if the excited state of interest was a pure excitation (i.e. HOMO → LUMO), or by explicitly calculating the excited state wavefunction from first principles.

6.3.3. *Many-body perturbation theory*

In the previous two sections, we have discussed approaches which aim at addressing some of the many-body effects neglected in the single-particle approximation. We have demonstrated that TDDFT offers an accurate and computationally efficient approach for simulating pre-edges, however as a consequence of

approximations within the *x–c* functional (f_{xc}), it is unable to account for strong electron correlation effects such as multiplets. These problems can be solved using post Hartree-Fock methods. However, these approaches are computationally expensive and unless a cluster model is used [338], are at present excluded for solids.

Besides wavefunction and density functional based approaches, the description of electronic excitations may also be achieved using many-body perturbation theory, by solving the Bethe–Salpeter equation (BSE) [345]. Loosely speaking, this approach has similar characteristics to TDDFT [346,347], and like Eq. (10), may also be expressed as a Dyson-like equation. However, a number of key differences exist (see Ref. [347] for a detailed discussion). In particular, the BSE involves the propagation of two particles (electron and hole) and naturally incorporates particle–hole interactions often required to simulate the fine spectral details of an XAS spectrum. Such interactions require a non-local and frequency dependent screened interaction of the electron–hole pair and therefore are not described within TDDFT by the vast majority of *x–c* functionals.

Vinson et al. [289,348] have recently presented such an approach for core-hole excitations. In their approach, the potential was based upon Kohn-Sham orbitals within a plane-wave basis [268] and then corrected with a self-energy calculated within Hedins GW approximation and modelled using the many pole self-energy (MPSE) model [55]. The spectrum is then calculated using the core-level BSE approach of Shirley [349,350]. While more computationally challenging than TDDFT, the inclusion of non-local and multiplet effects is important and using it the authors showed excellent agreement with experiment for a range of periodic lattices. Indeed, their simulations highlighted not only the limitations of the MT approximation, but also the role of many-body effects and the improvements brought about by the MPSE approach [55]. This has also been applied to simulate the $L_{2/3}$-edge spectra of several transition metals with various 3d occupations [348] and to study the core-hole spectra of liquid and solid water [351].

6.4. The geometric structure: The EXAFS region

The challenge in obtaining a quantitative description of the XANES region of the spectrum has made the EXAFS region more attractive for a structural analysis. In this region, typically >50 eV above the absorption edge, the photoelectron is not sensitive to the fine details of the potential and the many-body effects can be accounted for in a phenomenological manner. Thus, this region can be simulated using the EXAFS equation [59,256,48]:

$$\chi(k) = \sum_{\gamma} \frac{N_\gamma S_0^2 |f_{eff}(k)|}{kR_\gamma^2} \exp^{-2R_\gamma/\lambda_{tot}(k)} \exp^{-2\sigma^2 k^2} \sin(2kR_\gamma + \phi_\gamma). \quad (14)$$

Here, γ is the scattering path index with degeneracy N_γ. The half-path distance and the squared Debye-Waller (DW) factor are represented by R_γ and σ^2, respectively. In addition, $f_{eff}(k) = |f(k)| \exp^{i\phi(k)}$ is the complex backscattering amplitude for path γ, ϕ_γ is the central atom phase shift of the final state and λ_{tot}(k) is the energy-dependent mean free path. S_0^2 is the overall amplitude reduction factor which accounts for many-body effects.

Traditionally, the initial step in obtaining a qualitative description of the structure is achieved by a Fourier transform of the EXAFS signal in *k*-space [352] which yields a pseudo-radial distribution. However for systems containing many scattering pathways, which contribute to the same region of *R*-space, an unambiguous assignment of the peaks can be difficult.

To overcome this, Funke and co-workers [353,354] developed an approach based on a Wavelet transform (WT). This multi-resolution analysis enables interpretation of the spectrum as a function of *k*- and *R*, concurrently, yielding a 2D correlation plot in both coordinates (analogous to a time-frequency correlation plot). Owing to the *k*-dependence of the back-scattering amplitude [355], it separates the contributions between different scattering pathways at the same distance from the absorbing atom and between the contributions of single- and multiple-scattering events. The WT is expressed as:

$$W_f^{\psi}(a, k\prime) = \frac{1}{\sqrt{a}} \int_{-\infty}^{\infty} \chi(k) \psi^* \left(\frac{k - k\prime}{a} \right) dk, \quad (15)$$

where the scalar product of the EXAFS signal and the complex conjugate of the wavelet (ψ^*) is calculated as a function of a and k'. a is the scaling function, connected to *R*-space through the relation $a = \eta/2R$ and k' corresponds to the translation of the original wavelet as a function of the *k*-vector. We have recently implemented this method to the case of molecular systems [356] and applied it to study $[Fe(CN)_6]^{4-}$ and $[ReBr(CO)_3bpy]$. Our results highlighted the importance of multiple scattering, and both single and multiple scattering pathways and their relative contributions could be individually assigned. We also shed light on the low sensitivity of the EXAFS spectrum to the Re-halide scattering pathway [201].

Fig. 18 shows the WT approach applied to the Ti K-edge EXAFS spectrum of anatase titanium dioxide (TiO_2) nanoparticles [204]. TiO_2, in its anatase crystalline form, is the most promising metal oxide semiconductor for applications in photocatalysis and solar energy conversion. The crystalline structure of these nanoparticles gives rise to many overlapping scattering pathways which can be distinguished using the WT approach. The principle contribution derives from the O–Ti scattering of the first coordination sphere around the absorbing Ti. Indeed, this approach shows a main peak, with a small shoulder, highlighting the D_{2d} structure of anatase TiO_2 coordination. The latter is not visible in the Fourier transform. At larger values of R, the Ti–Ti scattering pathway is observed. In addition, multiple-scattering contributions (O–O–Ti and Ti–O–Ti) are found at larger *k*-values owing to enhanced back-scattering amplitudes at these *k*-values [355].

This approach offers an interesting alternative approach to analyse EXAFS spectra. While still in its infancy, developments should include a fitting procedure, which one could expect will offer a more detailed and unambiguous description of the molecular structure from the EXAFS spectrum. Finally in the context of this review it should also be extended into the time-domain XAS, for which changes in the WT could be directly associated with changes of the structure, offering many potentially exciting opportunities, especially given the significant improvement in S/N associated with the previously described experimental developments.

6.5. Simulation of ultrafast dynamics

6.5.1. X-ray spectroscopy

The temporal resolution of 3rd-generation storage rings (~ 50–100 ps) means that results are usually *quasi-static*. Therefore the experiment probes a metastable state, while the response of the system and surrounding environment occurs within the temporal width of the X-rays and consequently can be neglected in the simulations. For sub-picosecond X-ray absorption spectra, this picture breaks down and the evolving nuclear dynamics [357] and response of the environment must be addressed. For the latter this can be accounted for using molecular dynamics [358–363]. However, for the former, explicitly simulating the excited state dynamics of the solute, especially when nonadiabatic effects (i.e. breakdown of the Born-Oppenheimer approximation) are important is non-trivial.

The excited state dynamics can be studied using either an explicit description of all nuclear degrees of freedom or a model

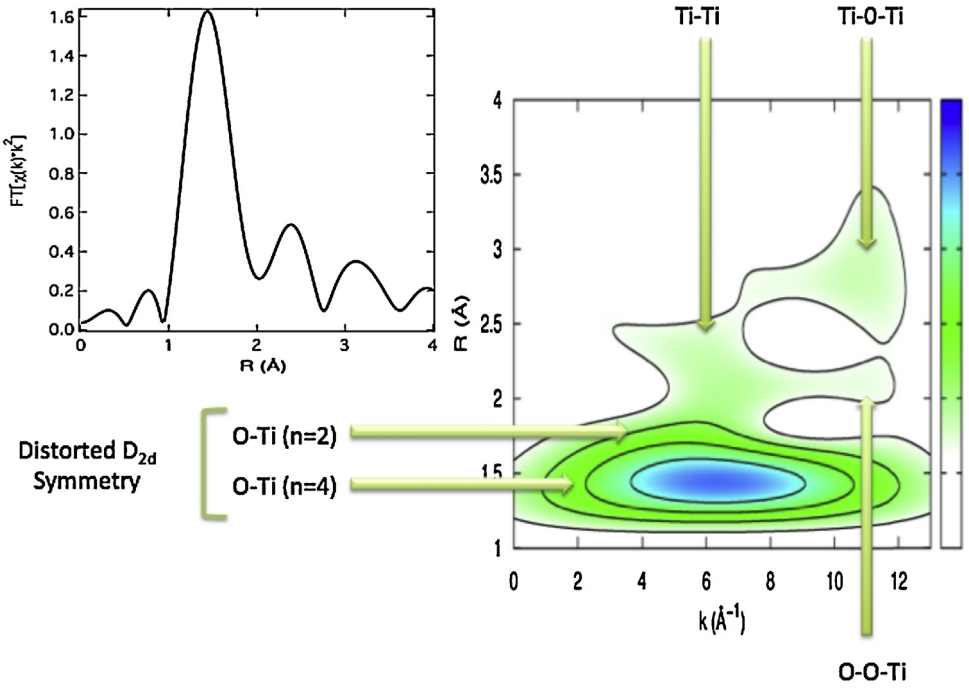

Fig. 18. The Fourier transform (upper left) and Wavelet transform of the EXAFS spectrum of anatase TiO_2 nanoparticles. The important scattering pathways are highlighted.

Hamiltonian. The former typically uses an approximate classical treatment of the nuclear dynamics, and nonadiabatic effects are incorporated using Tully's trajectory surface hopping approach [364]. Here, owing to the spatially local trajectories, full configurational space dynamics are achieved *on-the-fly* as the potential is calculated for a given nuclear configuration as and when it is required. This has led to these approaches being implemented with a wide range of electronic-structure methods [365,366]. For larger systems, the major constraint is the computational expense of the electronic structure method used and therefore, excited state molecular dynamics formulated within the framework of time-dependent density functional theory [367–373] is particularly appealing. This approach was recently used to study the ultrafast nonadiabatic dynamics of $[Ru(bpy)_3]^{2+}$ in water [372], for which the environment was explicitly included within the quantum mechanics/molecular mechanics (QM/MM) framework. The authors found excellent agreement for the intersystem crossing rate with previous experimental observations [374]. Alternative approaches have been proposed by Prezhdo and co-workers [375,376]. Here instead of explicitly solving the TDDFT equations, the excited states are represented as the energy difference between the Kohn-Sham orbitals occupied in the ground and excited sates. This makes it easier to simulate very large (in terms of both nuclear and electronic degrees of freedom) systems such charge transfer processes at metal-oxide interfaces [377]. However, the representation of the excited states is not rigorous, and therefore the description of the potential and the coupling between them cannot be improved systematically.

For such molecular dynamics approaches, the principle drawbacks are the neglect of quantum nuclear effects and that many trajectories are required to capture all of the possible relaxation pathways and to achieve statistical relevance. An alternative approach is to perform nuclear quantum dynamics, such as the Multi-Configurational Time-Dependent Hartree (MCTDH) method [378]. In contrast to standard quantum dynamics approaches, the MCTDH wavefunction *ansatz* uses a time-dependent basis. These basis functions have two principle advantages: (1) Fewer basis function are required as they are variationally determined. (2) The functions can be multi-dimensional particles containing more then one degree of freedom reducing the effective number of degree of freedom [379]. Using this approach, simulations can achieve ~50 nuclear degrees of freedom and using the multi-layer variant [380] dynamics have been performed with over 1000 nuclear degrees of freedom [381]. In contrast to excited state molecular dynamics, these approaches rigorously include quantum nuclear effects, however usually require [382,383] that the potential is pre-calculated and therefore model Hamiltonians are typically used in which only the most important degrees of freedom are included. In the case that the dynamics are driven by only a few dominant degrees of freedom, accurate Hamiltonians can easily be constructed [384], alternatively for larger more complicated systems more involved approaches are required [377,385,386].

6.5.2. The nonlinear regime

As previously discussed, the large peak brightness of the X-FELs offers new possibilities for non-linear core-level spectroscopies. In the simplest case the presently applied second-order spectroscopes are enhanced by the stimulated X-ray Raman process. Here, the probe pulse that excites a core electron also causes the stimulated emission of a photon offering large gains in the emission intensity [249,387].

Alternatively, Mukamel and co-workers have worked extensively on proposing new non-linear experiments with X-FEL pulses involving X-ray pump and probe. For 1D impulsive stimulated X-ray Raman spectroscopies (1D-SXRS) [388–390,57,391], an X-ray pulse excites a core electron to an unoccupied orbital. The core-hole is then filled emitting a photon with a given energy transfer (Ω–ω) to the system. This creates an excitation within the system which is then probed using a second X-ray pulse, at variable time-delay. This approach extends the applicability of RIXS and in particular owing to the local nature of core-excitations, by tuning the two pulses to different core-excitations within the system it becomes possible to prepare a wavepacket around one atom and probed at another. This has recently been applied to simulate the energy transfer in metalloporphyrin heterodimers during a time-delay of 50 fs [392]. The authors demonstrated that the time-dependent signal can reveal an oscillatory electron

transfer between the two dimers in this model system. The effect of nuclear motion has also recently been investigated [391]. The same authors have also recently extended this approach into a multidimensional technique involving the interaction with three X-ray pulses [389,393]. However experimentally issues of sample damage from irradiation by high intensity X-ray pulses will have to be dealt with. The developments with the VUV FELs [255] will pave the way for experiments in the hard X-ray regime.

7. Summary and outlook

In this contribution we have reviewed the most recent developments in X-ray spectroscopies and in the accompanying theories with a particular focus on applications to time-resolved studies. In the area of experiments, the high-repetition rate ps XAS/XES and the fs XAS experiments at X-FELs are the most important developments. It is clear that the ability to measure high-quality signal-to-noise ps transient XAS represents a significant improvement over previous efforts. The fact that the high repetition rate ps pump laser systems are robust and compact has made them a popular choice for implementation at pre-existing beamlines, as well as being used in temporary experimental setups at highly specialised beamlines. Several facilities, including the Stanford Synchrotron Radiation Light source and the Beijing Synchrotron Radiation Facility, are working on further implementing high-repetition rate techniques. Recently Navirian et al. [394] introduced a high-repetition rate setup at BESSY II using X-ray diffraction as the sample probe, emphasising the diversity possible at a storage ring facility. Picosecond XAS will remain a major tool for decades to come, even after the proliferation of X-FELs. Scientifically, there are still a host of issues to understand prior to going into the fs time domain. They also offer a better flexibility to test systems prior to experiments at FELs. They therefore represent complementary tools to femtosecond XAS/XES measurements performed at slicing sources and X-FELs in the future [178]. It is interesting to note that most of the studies based on ps high repetition rate XAS or femtosecond XAS at X-FELs have so far dealt with coordination chemistry complexes. Not only for benchmarking these new schemes, but also this is an area where the need for such sources is most important, as time-domain X-ray spectroscopies have shown their potential to answer scientific questions that no other experimental tool could so far address.

As regards theory, the last decade has witnessed huge advances in approaches for calculating core hole spectra. One-particle/one-hole approaches, such as TDDFT, can now routinely obtain at least a qualitative description of the pre-edge region and the continuing development of new functionals and kernels offers a bright future for density functional based approaches. When spin orbit coupling and multiplet effects are important, higher levels of theory such as post-Hartree-Fock approaches can now be used. Importantly, these developments means that a hierarchy of computational approaches for tackling core hole excitations is now evolving and the range of methods available offer a balance between accuracy and computational expensive meaning that it is possible to tackle a wide range of chemically interesting problems. The advent of femtosecond core-level spectroscopy means that dynamical effects can no longer be neglected and to achieve a full understanding of experimental data the excited state electronic and nuclear dynamics must be explicitly calculated. The best approach for this remains, at present, an open question.

Acknowledgements

We thank all of our coworkers over the years on the various ultrafast XAS studies. This work was funded by the Swiss NSF through the NCCR MUST 'Molecular ultrafast science and technology' and via contracts 200020-135502, 200021-137596, 200021-144517and 200021-137717. The X-ray measurements shown in Fig. 4 were measured at the SuperXAS beamline of the Swiss Light Source (Paul Scherrer Institut).

References

[1] A.H. Zewail, Science 242 (1988) 1645.
[2] A.H. Zewail, J. Phys. Chem. A 104 (2000) 5660.
[3] S. Mukamel, Principles of Nonlinear Optical Spectroscopy, Oxford University Press, USA, 1995.
[4] D.A. Reis, A.M. Lindenberg, Top. Appl. Phys. 108 (2007) 371.
[5] T. Elsaesser, M. Woerner, Acta Crystallogr. A 66 (2010) 168.
[6] S.L. Johnson, P. Beaud, E. Vorobeva, C.J. Milne, E.D. Murray, S. Fahy, G. Ingold, Acta Crystallogr. A 66 (2010) 157.
[7] A. Zewail, Annu. Rev. Phys. Chem. 57 (2006) 65.
[8] G. Sciaini, R.J.D. Miller, Rep. Prog. Phys. 74 (2011) 096101.
[9] F. Carbone, P. Musumeci, O. Luiten, C. Hebert, Chem. Phys. 392 (2012) 1.
[10] M. Chergui, A.H. Zewail, ChemPhysChem 10 (2009) 28.
[11] T. Penfold, C. Milne, M. Chergui, Adv. Chem. Phys. 153 (2013) 1.
[12] C. Bressler, R. Abela, M. Chergui, Z. Kristallogr. 223 (2008) 308.
[13] C. Bressler, M. Chergui, Annu. Rev. Phys. Chem. 61 (2010) 263.
[14] L. Chen, Annu. Rev. Phys. Chem. 56 (2005) 221.
[15] L. Chen, J. Electron Spectrosc. Relat. Phenom. 119 (2001) 161.
[16] W. Gawelda, A. Cannizzo, V.-T. Pham, A. El Nahhas, C.J. Milne, R. van der Veen, C. Bressler, M. Chergui, Chimia 61 (2007) 179.
[17] M. Chergui, Acta Crystallogr. A 66 (2010) 229.
[18] L.X. Chen, G. Jennings, T. Liu, D. Gosztola, J. Hessler, D. Scaltrito, G. Meyer, J. Am. Chem. Soc. 124 (2002) 10861.
[19] L. Chen, G. Shaw, I. Novozhilova, T. Liu, G. Jennings, K. Attenkofer, G. Meyer, P. Coppens, J. Am. Chem. Soc. 125 (2003) 7022.
[20] L.X. Chen, X. Zhang, J.V. Lockard, A.B. Stickrath, K. Attenkofer, G. Jennings, D.-J. Liu, Acta Crystallogr. A 66 (2010) 240.
[21] L.X. Chen, Annu. Rev. Phys. Chem. 56 (2005) 221.
[22] L. Chen, Angew. Chem. Int. Ed. 43 (2004) 2886.
[23] W. Gawelda, M. Johnson, F.M.F. de Groot, R. Abela, C. Bressler, M. Chergui, J. Am. Chem. Soc. 128 (2006) 5001.
[24] W. Gawelda, C. Bressler, M. Saes, M. Kaiser, A.N. Tarnovsky, D. Grolimund, S.L. Johnson, R. Abela, M. Chergui, Phys. Scr. T 115 (2005) 102.
[25] W. Gawelda, V.T. Pham, R.M. van der Veen, D. Grolimund, R. Abela, M. Chergui, C. Bressler, J. Chem. Phys. 130 (2009) 124520.
[26] W. Gawelda, V. Pham, M. Benfatto, Y. Zaushitsyn, M. Kaiser, D. Grolimund, S. Johnson, R. Abela, A. Hauser, C. Bressler, M. Chergui, Phys. Rev. Lett. 98 (2007) 057401.
[27] V.-T. Pham, W. Gawelda, Y. Zaushitsyn, M. Kaiser, D. Grolimund, S.L. Johnson, R. Abela, C. Bressler, M. Chergui, J. Am. Chem. Soc. 129 (2007) 1530.
[28] M. Saes, C. Bressler, R. Abela, D. Grolimund, S. Johnson, P. Heimann, M. Chergui, Phys. Rev. Lett. 90 (2003) 047403.
[29] M. Khalil, M.A. Marcus, A.L. Smeigh, J.K. McCusker, H.H.W. Chong, R.W. Schoenlein, J. Phys. Chem. A 110 (2006) 38.
[30] N. Huse, M. Khalil, T.K. Kim, A.L. Smeigh, L. Jamula, J.K. McCusker, R.W. Schoenlein, JPCS 148 (2009) 012043.
[31] N. Huse, T.K. Kim, L. Jamula, J.K. McCusker, F.M.F. de Groot, R.W. Schoenlein, J. Am. Chem. Soc. 132 (2010) 6809.
[32] X. Zhang, G. Smolentsev, J. Guo, K. Attenkofer, C. Kurtz, G. Jennings, J.V. Lockard, A.B. Stickrath, L.X. Chen, J. Phys. Chem. Lett. 2 (2011) 628.
[33] C. Milne, R. van der Veen, V. Pham, F. Lima, H. Rittmann-Frank, M. Reinhard, F. van Mourik, S. Karlsson, T. Penfold, M. Chergui, Chimia 65 (2011) 303.
[34] S.L. Johnson, P.A. Heimann, A.M. Lindenberg, H. Jeschke, M.E. Garcia, Z. Chang, R.W. Lee, J. Rehr, R.W. Falcone, Phys. Rev. Lett. 91 (2003) 157403.
[35] S.L. Johnson, P.A. Heimann, A.G. Macphee, A.M. Lindenberg, O.R. Monteiro, Z. Chang, R.W. Lee, R.W. Falcone, Phys. Rev. Lett. 94 (2005) 4.
[36] E. Vorobeva, S.L. Johnson, P. Beaud, C.J. Milne, M. Benfatto, G. Ingold, Phys. Rev. B 80 (2009) 134301.
[37] J.E. Katz, B. Gilbert, X. Zhang, K. Attenkofer, R.W. Falcone, G.A. Waychunas, J. Phys. Chem. Lett. 1 (2010) 1372.
[38] A. Zholents, M.S. Zolotorev, Phys. Rev. Lett. 76 (1996) 912.
[39] R.W. Schoenlein, S. Chattopadhyay, H.H.W. Chong, T.E. Glover, P.A. Heimann, C. Shank, A. Zholents, M.S. Zolotorev, Science 287 (2000) 2237.
[40] S. Khan, K. Holldack, T. Kachel, R. Mitzner, T. Quast, Phys. Rev. Lett. 97 (2006) 074801.
[41] P. Beaud, S. Johnson, A. Streun, R. Abela, D. Abramsohn, D. Grolimund, F. Krasniqi, T. Schmidt, V. Schlott, G. Ingold, Phys. Rev. Lett. 99 (2007) 174801.
[42] M. Abo-Bakr, J. Feikes, K. Holldack, P. Kuske, W. Peatman, U. Schade, G. Wustefeld, H. Hubers, Phys. Rev. Lett. 90 (2003) 094801.
[43] J. Feikes, K. Holldack, P. Kuske, G. Wustefeld, Proceedings of EPAC 2004, Lucerne, Switzerland, 2004.
[44] C. Bressler, C. Milne, V.T. Pham, A. ElNahhas, R.M. van der Veen, W. Gawelda, S. Johnson, P. Beaud, D. Grolimund, M. Kaiser, C.N. Borca, G. Ingold, R. Abela, M. Chergui, Science 323 (2009) 489.
[45] V.-T. Pham, T.J. Penfold, R.M. van der Veen, F. Lima, A. el Nahhas, S.L. Johnson, P. Beaud, R. Abela, C. Bressler, I. Tavernelli, C.J. Milne, M. Chergui, J. Am. Chem. Soc. 133 (2011) 12740.

[46] N. Huse, H. Cho, K. Hong, L. Jamula, F. de Groot, T. Kim, J. McCusker, R. Schoenlein, J. Phys. Chem. Lett. 2 (2011) 880.
[47] H.T. Lemke, C. Bressler, L.X. Chen, D.M. Fritz, K.J. Gaffney, A. Galler, W. Gawelda, K. Haldrup, R.W. Hartsock, H. Ihee, J. Kim, K.H. Kim, J.H. Lee, M.M. Nielsen, A.B. Stickrath, W. Zhang, D. Zhu, M. Cammarata, J. Phys. Chem. A 117 (2013) 735.
[48] J. Rehr, Rev. Mod. Phys. 72 (2000) 621.
[49] d. Groot, Coord. Chem. Rev. 249 (2005) 31.
[50] F. de Groot, A. Kotani, Core Level Spectroscopy of Solids, CRC Press, Boca Raton, 2008.
[51] S. Coriani, O. Christiansen, T. Fransson, P. Norman, Phys. Rev. A 85 (2012) 022507.
[52] I. Josefsson, K. Kunnus, S. Schreck, A. Föhlisch, F. de Groot, P. Wernet, M. Odelius, J. Phys. Chem. Lett. (2012) 3565.
[53] M. Roemelt, F. Neese, J. Phys. Chem. A 117 (2013) 3069.
[54] C.R. Natoli, P. Krüger, K. Hatada, K. Hayakawa, D. Sébilleau, O. Šipr, J. Phys.: Condens. Matter 24 (2012) 365501.
[55] J. Kas, A. Sorini, M. Prange, L. Cambell, J. Soininen, J. Rehr, Phys. Rev. B 76 (2007) 195116.
[56] A. Ankudinov, Y. Takimoto, J. Rehr, Phys. Rev. B 71 (2005) 165110.
[57] S. Mukamel, D. Healion, Y. Zhang, J.D. Biggs, Annu. Rev. Phys. Chem. 64 (2013) 101.
[58] D.C. Koningsberger, R. Prins, X-ray Absorption: Principles, Applications, Techniques of EXAFS, SEXAFS, and XANES, Wiley-Interscience, New York, 1988.
[59] J. Stöhr, NEXAFS Spectroscopy, Volume 25 of Springer Series in Surface Sciences, Springer, Berlin, 1996.
[60] K. Hämälä inen, S. Manninen, J. Phys.: Condens. Matter 13 (2001) 7539.
[61] P. Glatzel, M. Sikora, G. Smolentsev, M. Fernandez-Garcia, Catal. Today 145 (2009) 294.
[62] U. Bergmann, P. Glatzel, Photosynth. Res. 102 (2009) 255.
[63] J. Goulon, C. Goulon-Ginet, R. Cortes, J.M. Dubois, J. Phys. I 43 (1982) 539.
[64] P. Glatzel, L. Jacquamet, U. Bergmann, F.M.F. de Groot, S.P. Cramer, Inorg. Chem. 41 (2002) 3121.
[65] J. Yano, Y. Pushkar, P. Glatzel, A. Lewis, K. Sauer, J. Messinger, U. Bergmann, V. Yachandra, J. Am. Chem. Soc. 127 (2005) 14974.
[66] H.A. Kramers, W. Heisenberg, Z. Phys. 31 (1925) 681.
[67] L.J.P. Ament, M. van Veenendaal, T.P. Devereaux, J.P. Hill, J. van den Brink, Rev. Mod. Phys. 83 (2011) 705.
[68] A. Kotani, S. Shin, Rev. Mod. Phys. 73 (2001) 203.
[69] F. de Groot, M.A. Arrio, P. Sainctavit, C. Cartier, C.T. Chen, Solid State Commun. 92 (1994) 991.
[70] R. Kurian, K. Kunnus, P. Wernet, S.M. Butorin, P. Glatzel, F.M.F. de Groot, J. Phys.: Condens. Matter 24 (2012) 452201.
[71] K. Hämälä inen, S. Manninen, P. Suortti, S.P. Collins, M.J. Cooper, D. Laundy, J. Phys.: Condens. Matter 1 (1989) 5955.
[72] U. Bergmann, C.R. Horne, T.J. Collins, J.M. Workman, S.P. Cramer, Chem. Phys. Lett. 302 (1999) 119.
[73] U. Bergmann, J. Bendix, P. Glatzel, H.B. Gray, S.P. Cramer, J. Chem. Phys. 116 (2002) 2011.
[74] V.A. Safonov, L.N. Vykhodtseva, Y.M. Polukarov, O.V. Safonova, G. Smolentsev, M. Sikora, S.G. Eeckhout, P. Glatzel, J. Phys. Chem. B 110 (2006) 23192.
[75] G. Smolentsev, A. Soldatov, J. Messinger, K. Merz, T. Weyhermuller, U. Bergmann, Y. Pushkar, J. Yano, V. Yachandra, P. Glatzel, J. Am. Chem. Soc. 131 (2009) 13161.
[76] M.U. Delgado-Jaime, B.R. Dible, K.P. Chiang, W.W. Brennessel, U. Bergmann, P.L. Holland, S. DeBeer, Inorg. Chem. 50 (2011) 10709.
[77] K.M. Lancaster, M. Roemelt, P. Ettenhuber, Y. Hu, M.W. Ribbe, F. Neese, U. Bergmann, S. DeBeer, Science 334 (2011) 974.
[78] C.J. Pollock, S. DeBeer, J. Am. Chem. Soc. 133 (2011) 5594.
[79] C.J. Pollock, K. Grubel, P.L. Holland, S. DeBeer, J. Am. Chem. Soc. 135 (2013) 11803.
[80] J. Szlachetko, M. Cotte, J. Morse, M. Salome, P. Jagodzinski, J.C. Dousse, J. Hoszowska, Y. Kayser, J. Susini, J. Synchrotron Radiat. 17 (2010) 400.
[81] F. Gel'mukhanov, H. Agren, Phys. Rep. 312 (1999) 87.
[82] P. Glatzel, M. Sikora, M. Fernández-García, Eur. Phys. J. Spec. Top. 169 (2009) 207.
[83] A. Kotani, K.O. Kvashnina, S.M. Butorin, P. Glatzel, Eur. Phys. J. B 85 (2012) 257.
[84] J. Kas, J. Rehr, J. Soininen, P. Glatzel, Phys. Rev. B 83 (2011) 235114.
[85] C. Vettier, Eur. Phys. J. Spec. Top. 208 (2012) 3.
[86] Y. Joly, S.D. Matteo, O. Bunău, Eur. Phys. J. Spec. Top. 208 (2012) 21.
[87] J. Fink, E. Schierle, E. Weschke, J. Geck, Rep. Prog. Phys. 76 (2013) 056502.
[88] J. Szlachetko, M. Nachtegaal, E. de Boni, M. Willimann, O. Safonova, J. Sa, G. Smolentsev, M. Szlachetko, J.A. van Bokhoven, J.C. Dousse, J. Hoszowska, Y. Kayser, P. Jagodzinski, A. Bergamaschi, B. Schmitt, C. David, A. Lücke, Rev. Sci. Instrum. 83 (2012) 103105.
[89] P. Glatzel, T.-C. Weng, K. Kvashnina, J. Swarbrick, M. Sikora, E. Gallo, N. Smolentsev, R.A. Mori, J. Electron Spectrosc. Relat. Phenom. 188 (2013) 17.
[90] D.A. Meyer, X. Zhang, U. Bergmann, K.J. Gaffney, J. Chem. Phys. 132 (2010) 134502.
[91] E. Gallo, F. Bonino, J.C. Swarbrick, T. Petrenko, A. Piovano, S. Bordiga, D. Gianolio, E. Groppo, F. Neese, C. Lamberti, P. Glatzel, ChemPhysChem 14 (2013) 79.
[92] E. Gallo, C. Lamberti, P. Glatzel, Inorg. Chem. 52 (2013) 5633.
[93] K. Hämälä inen, D.P. Siddons, J.B. Hastings, L.E. Berman, Phys. Rev. Lett. 67 (1991) 2850.
[94] A. Kotani, Eur. Phys. J. B 47 (2005) 3.
[95] S. Huotari, T. Pylkkänen, G. Vanko, R. Verbeni, P. Glatzel, G. Monaco, Phys. Rev. B 78 (2008) 041102.
[96] L. Braicovich, J. van den Brink, V. Bisogni, M.M. Sala, L.J.P. Ament, N.B. Brookes, G.M. De Luca, M. Salluzzo, T. Schmitt, V.N. Strocov, G. Ghiringhelli, Phys. Rev. Lett. 104 (2010) 077002.
[97] H. Yavas, M. van Veenendaal, J. van den Brink, L.J.P. Ament, A. Alatas, B.M. Leu, M.-O. Apostu, N. Wizent, G. Behr, W. Sturhahn, H. Sinn, E.E. Alp, J. Phys.: Condens. Matter 22 (2010) 485601.
[98] P. Wernet, K. Kunnus, S. Schreck, W. Quevedo, R. Kurian, S. Techert, F.M.F. de Groot, M. Odelius, A. Föhlisch, J. Phys. Chem. Lett. 3 (2012) 3448.
[99] P. Carra, M. Fabrizio, B.T. Thole, Phys. Rev. Lett. 74 (1995) 3700.
[100] F. de Groot, Chem. Rev. 101 (2001) 1779.
[101] F. De Groot, M. Krisch, J. Vogel, Phys. Rev. B 66 (2002) 195112.
[102] J.C. Swarbrick, U. Skyllberg, T. Karlsson, P. Glatzel, Inorg. Chem. 48 (2009) 10748–10756.
[103] O.V. Safonova, M. Tromp, J.A. van Bokhoven, F.M.F. de Groot, J. Evans, P. Glatzel, J. Phys. Chem. B 110 (2006) 16162.
[104] H. Hayashi, Y. Udagawa, W.A. Caliebe, C.-C. Kao, Chem. Phys. Lett. 371 (2003) 125.
[105] R.M. van der Veen, J.J. Kas, C.J. Milne, V.-T. Pham, A. el Nahhas, F.A. Lima, D.A. Vithanage, J.J. Rehr, R. Abela, M. Chergui, PCCP 12 (2010) 5551.
[106] M. Kavčič, M. Žitnik, K. Bučar, A. Mihelič, B. Marolt, J. Szlachetko, P. Glatzel, K. Kvashnina, Phys. Rev. B 87 (2013) 075106.
[107] J. Szlachetko, M. Nachtegaal, J. Sa, J.-C. Dousse, J. Hoszowska, E. Kleymenov, M. Janousch, O.V. Safonova, C. König, J.A. van Bokhoven, Chem. Commun. 48 (2012) 10898.
[108] P. Eisenberger, P.M. Platzman, H. Winick, Phys. Rev. Lett. 36 (1976) 623.
[109] J. Tulkki, T. Aberg, J. Phys. B 15 (1982) L435.
[110] N. Zhavoronkov, Y. Gritsai, M. Bargheer, M. Woerner, T. Elsaesser, F. Zamponi, I. Uschmann, E. Förster, Opt. Lett. 30 (2005) 1737.
[111] C. Reich, C.M. Laperle, X. Li, B. Ahr, F. Benesch, C.G. Rose-Petruck, Opt. Lett. 32 (2007) 427.
[112] C. Rose-Petruck, R. Jimenez, T. Guo, A. Cavalleri, C.W. Siders, F. Rksi, J.A. Squier, B.C. Walker, K.R. Wilson, C.P. Barty, Nature 398 (1999) 310.
[113] U. Shymanovich, M. Nicoul, W. Lu, S. Kähle, A. Tarasevitch, K. Sokolowski-Tinten, D. von der Linde, Rev. Sci. Instrum. 80 (2009) 083102.
[114] C.W. Siders, A. Cavalleri, K. Sokolowski-Tinten, C. Tóth, T. Guo, M. Kammler, M.H.v. Hoegen, K.R. Wilson, D.v.d. Linde, C.P.J. Barty, Science 286 (1999) 1340.
[115] A. Oguz Er, J. Chen, P.M. Rentzepis, J. Appl. Phys. 112 (2012) 031101.
[116] B. Freyer, F. Zamponi, V. Juvé, J. Stingl, M. Woerner, T. Elsaesser, M. Chergui, J. Chem. Phys. 138 (2013) 144504.
[117] F. Raksi, K. Wilson, Z. Jiang, A. Ikhlef, C. Cote, J.-C. Kieffer, J. Chem. Phys. 104 (1996) 6066.
[118] J. Chen, H. Zhang, I.V. Tomov, X. Ding, P.M. Rentzepis, Chem. Phys. Lett. 437 (2007) 50.
[119] W. Fullagar, M. Harbst, S. Canton, J. Uhlig, M. Walczak, C.G. Wahlström, V. Sundstrom, Rev. Sci. Instrum. 78 (2007) 115105.
[120] C. Bonté, M. Harmand, F. Dorchies, S. Magnan, V. Pitre, J.-C. Kieffer, P. Audebert, J.P. Geindre, Rev. Sci. Instrum. 78 (2007) 043503.
[121] J. Uhlig, W. Fullagar, J.N. Ullom, W.B. Doriese, J.W. Fowler, D.S. Swetz, N. Gador, S.E. Canton, K. Kinnunen, I.J. Maasilta, C.D. Reintsema, D.A. Bennett, L.R. Vale, G.C. Hilton, K.D. Irwin, D.R. Schmidt, V. Sundstrom, Phys. Rev. Lett. 110 (2013) 138302.
[122] F. Grüner, S. Becker, U. Schramm, T. Eichner, M. Fuchs, R. Weingartner, D. Habs, J. Meyer-Ter-Vehn, M. Geissler, M. Ferrario, L. Serafini, B. van der Geer, H. Backe, W. Lauth, S. Reiche, Appl. Phys. B 86 (2007) 431.
[123] P.B. Corkum, Phys. Rev. Lett. 71 (1993) 1994.
[124] M. Drescher, M. Hentschel, R. Kienberger, G. Tempea, C. Spielmann, G.A. Reider, P.B. Corkum, F. Krausz, Science 291 (2001) 1923.
[125] T. Pfeifer, C. Spielmann, G. Gerber, Rep. Prog. Phys. 69 (2006) 443.
[126] Z.-H. Loh, S.R. Leone, J. Phys. Chem. Lett. 4 (2013) 292.
[127] E.R. Hosler, S.R. Leone, Phys. Rev. A 88 (2013) 023420.
[128] M. Faubel, K.R. Siefermann, Y. Liu, B. Abel, Acc. Chem. Res. 45 (2012) 120.
[129] K. Siefermann, Y. Liu, E. Lugovoy, O. Link, M. Faubel, U. Buck, B. Winter, B. Abel, Nat. Chem. 2 (2010) 274.
[130] R. Berlasso, C. Dallera, F. Borgatti, C. Vozzi, G. Sansone, S. Stagira, M. Nisoli, G. Ghiringhelli, P. Villoresi, L. Poletto, M. Pascolini, S. Nannarone, S. De Silvestri, L. Braicovich, Phys. Rev. B 73 (2006) 115101.
[131] J. Vura-Weis, C.-M. Jiang, C. Liu, H. Gao, J.M. Lucas, F.M.F. de Groot, P. Yang, A.P. Alivisatos, S.R. Leone, J. Phys. Chem. Lett. (2013) 3667.
[132] G. Margaritondo, J. Synchrotron Radiat. 2 (1995) 148.
[133] P. Wilmott, An Introduction to Synchrotron Radiation:Techniques and Applications, Wiley, Chichester, 2011.
[134] T. Ishikawa, K. Tamasaku, M. Yabashi, Nucl. Instrum. Meth. A 547 (2005) 42.
[135] M. Krisch, F. Sette, Top. Appl. Phys. 108 (2007) 317.
[136] A. Iida, K. Hirano, Nucl. Instrum. Meth. B 114 (1996) 149.
[137] R. Kodama, N. Ikeda, Y. Kato, Y. Katori, T. Iwai, K. Takeshi, Opt. Lett. 21 (1996) 1321.
[138] M. Yabashi, J.B. Hastings, M.S. Zolotorev, H. Mimura, H. Yumoto, S. Matsuyama, K. Yamauchi, T. Ishikawa, Phys. Rev. Lett. 97 (2006) 4.
[139] T. Katayama, Y. Inubushi, Y. Obara, T. Sato, T. Togashi, K. Tono, T. Hatsui, T. Kameshima, A. Bhattacharya, Y. Ogi, N. Kurahashi, K. Misawa, T. Suzuki, M. Yabashi, Appl. Phys. Lett. 103 (2013) 131105.
[140] S. Pascarelli, O. Mathon, M. Munoz, T. Mairs, J. Susini, J. Synchrotron Radiat. 13 (2006) 351.

[141] M. Tromp, A.J. Dent, J. Headspith, T.L. Easun, X.-Z. Sun, M.W. George, O. Mathon, G. Smolentsev, M.L. Hamilton, J. Evans, J. Phys. Chem. B 117 (2013) 7381.
[142] Y. Obara, T. Katayama, Y. Ogi, T. Suzuki, N. Kurahashi, S. Karashima, Y. Chiba, Y. Isokawa, T. Togashi, Y. Inubushi, M. Yabashi, T. Suzuki, K. Misawa, Opt. Lett. 22 (2014) 1105.
[143] M. Saes, C. Bressler, F. van Mourik, W. Gawelda, M. Kaiser, M. Chergui, C. Bressler, D. Grolimund, R. Abela, T. Glover, P. Heimann, R. Schoenlein, S. Johnson, A. Lindenberg, R. Falcone, Rev. Sci. Instrum. 75 (2004) 24.
[144] D. Ferri, M.A. Newton, M. Nachtegaal, Top. Catal. 54 (2011) 1070.
[145] B. Sonntag, Nucl. Instrum. Meth. A 467 (2001) 8.
[146] C. Pellegrini, Rev. Accl. Sci. Tech. 03 (2010) 185.
[147] W.A. Barletta, J. Bisognano, J.N. Corlett, P. Emma, Z. Huang, K.J. Kim, R. Lindberg, J.B. Murphy, G.R. Neil, D.C. Nguyen, C. Pellegrini, R.A. Rimmer, F. Sannibale, G. Stupakov, R.P. Walker, A.A. Zholents, Nucl. Instrum. Meth. A 618 (2010) 69.
[148] P.R. Ribic, G. Margaritondo, J. Phys. D: Appl. Phys. 45 (2012) 213001.
[149] I.A. Vartanyants, A. Singer, A.P. Mancuso, O.M. Yefanov, A. Sakdinawat, Y. Liu, E. Bang, G.J. Williams, G. Cadenazzi, B. Abbey, H. Sinn, D. Attwood, K.A. Nugent, E. Weckert, T. Wang, D. Zhu, B. Wu, C. Graves, A. Scherz, J.J. Turner, W.F. Schlotter, M. Messerschmidt, J. Lüning, Y. Acremann, P. Heimann, D.C. Mancini, V. Joshi, J. Krzywinski, R. Soufli, M. Fernandez-Perea, S. Hau-Riege, A.G. Peele, Y. Feng, O. Krupin, S. Moeller, W. Wurth, Phys. Rev. Lett. 107 (2011) 144801.
[150] H.N. Chapman, A. Barty, M.J. Bogan, S. Boutet, M. Frank, S.P. Hau-Riege, S. Marchesini, B.W. Woods, S. Bajt, W.H. Benner, R.A. London, E. Plönjes, M. Kuhlmann, R. Treusch, S. Düsterer, T. Tschentscher, J.R. Schneider, E. Spiller, T. Möller, C. Bostedt, M. Hoener, D.A. Shapiro, K.O. Hodgson, D. van der Spoel, F. Burmeister, M. Bergh, C. Caleman, G. Huldt, M.M. Seibert, F.R.N.C. Maia, R.W. Lee, A. Szoke, N. Timneanu, J. Hajdu, Nat. Phys. 2 (2006) 839.
[151] H.N. Chapman, S.P. Hau-Riege, M.J. Bogan, S. Bajt, A. Barty, S. Boutet, S. Marchesini, M. Frank, B.W. Woods, W.H. Benner, R.A. London, U. Rohner, A. Szoke, E. Spiller, T. Möller, C. Bostedt, D.A. Shapiro, M. Kuhlmann, R. Treusch, E. Plönjes, F. Burmeister, M. Bergh, C. Caleman, G. Huldt, M.M. Seibert, J. Hajdu, Nature 448 (2007) 676.
[152] A. Barty, S. Boutet, M.J. Bogan, S. Hau-Riege, S. Marchesini, K. Sokolowski Tinten, N. Stojanovic, R. Tobey, H. Ehrke, A. Cavalleri, S. Duesterer, M. Frank, S. Bajt, B.W. Woods, M.M. Seibert, J. Hajdu, R. Treusch, H.N. Chapman, Nat. Photonics 2 (2008) 415.
[153] R.A. Kirian, X. Wang, U. Weierstall, K.E. Schmidt, J.C. Spence, M. Hunter, P. Fromme, T. White, H.N. Chapman, J. Holton, Opt. Express 18 (2010) 5713–5723.
[154] M.M. Seibert, T. Ekeberg, F.R.N.C. Maia, M. Svenda, J. Andreasson, O. Jönsson, D. Odić, B. Iwan, A. Rocker, D. Westphal, M. Hantke, D.P. Deponte, A. Barty, J. Schulz, L. Gumprecht, N. Coppola, A. Aquila, M. Liang, T.A. White, A. Martin, C. Caleman, S. Stern, C. Abergel, V. Seltzer, J.-M. Claverie, C. Bostedt, J.D. Bozek, S. Boutet, A.A. Miahnahri, M. Messerschmidt, J. Krzywinski, G. Williams, K.O. Hodgson, M.J. Bogan, C.Y. Hampton, R.G. Sierra, D. Starodub, I. Andersson, S. Bajt, M. Barthelmess, J.C.H. Spence, P. Fromme, U. Weierstall, R. Kirian, M. Hunter, R.B. Doak, S. Marchesini, S.P. Hau-Riege, M. Frank, R.L. Shoeman, L. Lomb, S.W. Epp, R. Hartmann, D. Rolles, A. Rudenko, C. Schmidt, L. Foucar, N. Kimmel, P. Holl, B. Rudek, B. Erk, A. Hömke, C. Reich, D. Pietschner, G. Weidenspointner, L. Strüder, G. Hauser, H. Gorke, J. Ullrich, I. Schlichting, S. Herrmann, G. Schaller, F. Schopper, H. Soltau, K.-U. Kühnel, R. Andritschke, C.-D. Schröter, F. Krasniqi, M. Bott, S. Schorb, D. Rupp, M. Adolph, T. Gorkhover, H. Hirsemann, G. Potdevin, H. Graafsma, B. Nilsson, H.N. Chapman, J. Hajdu, Nature 469 (2011) 78.
[155] H.N. Chapman, P. Fromme, A. Barty, T.A. White, R.A. Kirian, A. Aquila, M.S. Hunter, J. Schulz, D.P. Deponte, U. Weierstall, R.B. Doak, F.R.N.C. Maia, A.V. Martin, I. Schlichting, L. Lomb, N. Coppola, R.L. Shoeman, S.W. Epp, R. Hartmann, D. Rolles, A. Rudenko, L. Foucar, N. Kimmel, G. Weidenspointner, P. Holl, M. Liang, M. Barthelmess, C. Caleman, S. Boutet, M.J. Bogan, J. Krzywinski, C. Bostedt, S. Bajt, L. Gumprecht, B. Rudek, B. Erk, C. Schmidt, A. Hömke, C. Reich, D. Pietschner, L. Strüder, G. Hauser, H. Gorke, J. Ullrich, S. Herrmann, G. Schaller, F. Schopper, H. Soltau, K.-U. Kühnel, M. Messerschmidt, J.D. Bozek, S.P. Hau-Riege, M. Frank, C.Y. Hampton, R.G. Sierra, D. Starodub, G.J. Williams, J. Hajdu, N. Timneanu, M.M. Seibert, J. Andreasson, A. Rocker, O. Jönsson, M. Svenda, S. Stern, K. Nass, R. Andritschke, C.-D. Schröter, F. Krasniqi, M. Bott, K.E. Schmidt, X. Wang, I. Grotjohann, J.M. Holton, T.R.M. Barends, R. Neutze, S. Marchesini, R. Fromme, S. Schorb, D. Rupp, M. Adolph, T. Gorkhover, I. Andersson, H. Hirsemann, G. Potdevin, H. Graafsma, B. Nilsson, J.C.H. Spence, Nature 469 (2011) 73.
[156] J.N. Clark, X. Huang, R. Harder, I.K. Robinson, Nat. Commun. 3 (2012) 993.
[157] A. Barty, J. Küpper, H.N. Chapman, Annu. Rev. Phys. Chem. 64 (2013) 415.
[158] S. Lee, W. Roseker, C. Gutt, B. Fischer, H. Conrad, F. Lehmkühler, I. Steinke, D. Zhu, H. Lemke, M. Cammarata, D.M. Fritz, P. Wochner, M. Castro-Colin, S.O. Hruszkewycz, P.H. Fuoss, G.B. Stephenson, G. Grübel, A. Robert, Opt. Express 21 (2013) 24647.
[159] W.F. Schlotter, F. Sorgenfrei, T. Beeck, M. Beye, S. Gieschen, H. Meyer, M. Nagasono, A. Foehlisch, W. Wurth, Opt. Express 35 (2010) 372.
[160] A. Singer, F. Sorgenfrei, A.P. Mancuso, N. Gerasimova, O.M. Yefanov, J. Gulden, T. Gorniak, T. Senkbeil, A. Sakdinawat, Y. Liu, D. Attwood, S. Dziarzhytski, D.D. Mai, R. Treusch, E. Weckert, T. Salditt, A. Rosenhahn, W. Wurth, I.A. Vartanyants, Opt. Express 20 (2012) 17480.
[161] W. Ackermann, G. Asova, V. Ayvazyan, A. Azima, N. Baboi, J. Bähr, V. Balandin, B. Beutner, A. Brandt, A. Bolzmann, R. Brinkmann, O.I. Brovko, M. Castellano, P. Castro, L. Catani, E. Chiadroni, S. Choroba, A. Cianchi, J.T. Costello, D. Cubaynes, J. Dardis, W. Decking, H. Delsim-Hashemi, A. Delserieys, G. Di Pirro, M. Dohlus, S. Dusterer, A. Eckhardt, H.T. Edwards, B. Faatz, J. Feldhaus, K. Flöttmann, J. Frisch, L. Fröhlich, T. Garvey, U. Gensch, C. Gerth, M. Görler, N. Golubeva, H.J. Grabosch, M. Grecki, O. Grimm, K. Hacker, U. Hahn, J.H. Han, K. Honkavaara, T. Hott, M. Hüning, Y. Ivanisenko, E. Jaeschke, W. Jalmuzna, T. Jezynski, R. Kammering, V. Katalev, K. Kavanagh, E.T. Kennedy, S. Khodyachykh, K. Klose, V. Kocharyan, M. Körfer, M. Kollewe, W. Koprek, S. Korepanov, D. Kostin, M. Krassilnikov, G. Kube, M. Kuhlmann, C.L.S. Lewis, L. Lilje, T. Limberg, D. Lipka, F. Löhl, H. Luna, M. Luong, M. Martins, M. Meyer, P. Michelato, V. Miltchev, W.D. Möller, L. Monaco, W.F.O. Müller, O. Napieralski, O. Napoly, P. Nicolosi, D. Nölle, T. Nunez, A. Oppelt, C. Pagani, R. Paparella, N. Pchalek, J. Pedregosa-Gutierrez, B. Petersen, B. Petrosyan, G. Petrosyan, L. Petrosyan, J. Pflüger, E. Plönjes, L. Poletto, K. Pozniak, E. Prat, D. Proch, P. Pucyk, P. Radcliffe, H. Redlin, K. Rehlich, M. Richter, M. Roehrs, J. Roensch, R. Romaniuk, M. Ross, J. Rossbach, V. Rybnikov, M. Sachwitz, E.L. Saldin, W. Sandner, H. Schlarb, B. Schmidt, M. Schmitz, P. Schmüser, J.R. Schneider, E.A. Schneidmiller, S. Schnepp, S. Schreiber, M. Seidel, D. Sertore, A.V. Shabunov, C. Simon, S. Simrock, E. Sombrowski, A.A. Sorokin, P. Spanknebel, R. Spesyvtsev, L. Staykov, B. Steffen, F. Stephan, F. Stulle, H. Thom, K. Tiedtke, M. Tischer, S. Toleikis, R. Treusch, D. Trines, I. Tsakov, E. Vogel, T. Weiland, H. Weise, M. Wellhöfer, M. Wendt, I. Will, A. Winter, K. Wittenburg, W. Wurth, P. Yeates, M.V. Yurkov, I. Zagorodnov, K. Zapfe, Nat. Photonics 1 (2007) 336.
[162] K. Tiedtke, A. Azima, N. von Bargen, L. Bittner, S. Bonfigt, S. Duesterer, B. Faatz, U. Fruehling, M. Gensch, C. Gerth, N. Guerassimova, U. Hahn, T. Hans, M. Hesse, K. Honkavaar, U. Jastrow, P. Juranic, S. Kapitzki, B. Keitel, T. Kracht, M. Kuhlmann, W.B. Li, M. Martins, T. Nunez, E. Ploenjes, H. Redlin, E.L. Saldin, E.A. Schneidmiller, J.R. Schneider, S. Schreiber, N. Stojanovic, F. Tavella, S. Toleikis, R. Treusch, H. Weigelt, M. Wellhoefer, H. Wabnitz, M.V. Yurkov, J. Feldhaus, New J. Phys. 11 (2009) 023029.
[163] C. Bostedt, H.N. Chapman, J.T. Costello, J.R.C. Lopez-Urrutia, S. Duesterer, S.W. Epp, J. Feldhaus, A. Foehlisch, M. Meyer, T. Moeller, R. Moshammer, M. Richter, K. Sokolowski Tinten, A. Sorokin, K. Tiedtke, J. Ullrich, W. Wurth, Nucl. Instrum. Meth. A 601 (2009) 108–122.
[164] P. Emma, R. Akre, J. Arthur, R. Bionta, C. Bostedt, J. Bozek, A. Brachmann, P. Bucksbaum, R. Coffee, F.J. Decker, Y. Ding, D. Dowell, S. Edstrom, A. Fisher, J. Frisch, S. Gilevich, J. Hastings, G. Hays, P. Hering, Z. Huang, R. Iverson, H. Loos, M. Messerschmidt, A. Miahnahri, S. Moeller, H.D. Nuhn, G. Pile, D. Ratner, J. Rzepiela, D. Schultz, T. Smith, P. Stefan, H. Tompkins, J. Turner, J. Welch, W. White, J. Wu, G. Yocky, J. Galayda, Nat. Photonics 4 (2010) 641.
[165] J.D. Bozek, Eur. Phys. J. Spec. Top. 169 (2009) 129.
[166] J.M. Glownia, J. Cryan, J. Andreasson, A. Belkacem, N. Berrah, C.I. Blaga, C. Bostedt, J. Bozek, L.F. Dimauro, L. Fang, J. Frisch, O. Gessner, M. Gühr, J. Hajdu, M.P. Hertlein, M. Hoener, G. Huang, O. Kornilov, J.P. Marangos, A.M. March, B.K. McFarland, H. Merdji, V.S. Petrovic, C. Raman, D. Ray, D.A. Reis, M. Trigo, J.L. White, W. White, R. Wilcox, L. Young, R.N. Coffee, P.H. Bucksbaum, Opt. Express 18 (2010) 17620.
[167] S. Boutet, G.J. Williams, New J. Phys. 12 (2010) 035024.
[168] K. Kunnus, I. Rajkovic, S. Schreck, W. Quevedo, S. Eckert, M. Beye, E. Suljoti, C. Weniger, C. Kalus, S. Grübel, M. Scholz, D. Nordlund, W. Zhang, R.W. Hartsock, K.J. Gaffney, W.F. Schlotter, J.J. Turner, B. Kennedy, F. Hennies, S. Techert, P. Wernet, A. Föhlisch, Rev. Sci. Instrum. 83 (2012) 123109.
[169] A. Robert, R. Curtis, D. Flath, A. Gray, M. Sikorski, S. Song, V. Srinivasan, D. Stefanescu, JPCS 425 (2013) 212009.
[170] D. Pile, Nat. Photonics 5 (2011) 456.
[171] T. Ishikawa, H. Aoyagi, T. Asaka, Y. Asano, N. Azumi, T. Bizen, H. Ego, K. Fukami, T. Fukui, Y. Furukawa, S. Goto, H. Hanaki, T. Hara, T. Hasegawa, T. Hatsui, A. Higashiya, T. Hirono, N. Hosoda, M. Ishii, T. Inagaki, Y. Inubushi, T. Itoga, Y. Joti, M. Kago, T. Kameshima, H. Kimura, Y. Kirihara, A. Kiyomichi, T. Kobayashi, C. Kondo, T. Kudo, H. Maesaka, X.M. Maréchal, T. Masuda, S. Matsubara, T. Matsumoto, T. MATSUSHITA, S. Matsui, M. Nagasono, N. Nariyama, H. Ohashi, T. Ohata, T. Ohshima, S. Ono, Y. Otake, C. Saji, T. Sakurai, T. Sato, K. Sawada, T. Seike, K. Shirasawa, T. Sugimoto, S. Suzuki, S. Takahashi, H. Takebe, K. Takeshita, K. Tamasaku, H. Tanaka, R. Tanaka, T. Tanaka, T. Togashi, K. Togawa, A. Tokuhisa, H. Tomizawa, K. Tono, S. WU, M. Yabashi, M. Yamaga, A. Yamashita, K. Yanagida, C. Zhang, T. Shintake, H. Kitamura, N. Kumagai, Nat. Photonics 6 (2012) 540.
[172] M. Yabashi, H. Tanaka, T. Tanaka, H. Tomizawa, T. Togashi, M. Nagasono, T. Ishikawa, J.R. Harries, Y. Hikosaka, A. Hishikawa, K. Nagaya, N. Saito, E. Shigemasa, K. Yamanouchi, K. Ueda, J. Phys. B 46 (2013) 164001.
[173] E. Allaria, C. Callegari, D. Cocco, W.M. Fawley, M. Kiskinova, C. Masciovecchio, F. Parmigiani, New J Phys. 12 (2010) 075002.
[174] C. Svetina, N. Mahne, L. Raimondi, L. Rumiz, M. Zangrando, E. Allaria, F. Bencivenga, C. Callegari, F. Capotondi, D. Castronovo, P. Cinquegrana, P. Craievich, I. Cudin, M. Dal Forno, M.B. Danailov, G. D'Auria, R. De Monte, G. De Ninno, A. Demidovich, S. Di Mitri, B. Diviacco, A. Fabris, R. Fabris, W.M. Fawley, M. Ferianis, E. Ferrari, L. Froehlich, P. Furlan Radivo, G. Gaio, L. Giannessi, M. Kiskinova, M. Lonza, B. Mahieu, C. Masciovecchio, I.P. Nikolov, F. Parmigiani, E. Pedersoli, G. Penco, M. Predonzani, E. Principi, F. Rossi, C. Scafuri, C. Serpico, P. Sigalotti, S. Spampinati, C. Spezzani, M. Svandrlik, M. Trovo, A. Vascotto, M. Veronese, R. Visintini, D. Zangrando, in: A. Klisnick, C.S. Menoni (Eds.), SPIE Optical Engineering + Applications, SPIE, 2013, pp. 88490O-88490O–9.
[175] M. Altarelli, Nucl Instrum. Meth. B 269 (2011) 2845.
[176] M. Fuchs, R. Weingartner, A. Popp, Z. Major, S. Becker, J. Osterhoff, I. Cortrie, B. Zeitler, R. Hörlein, G.D. Tsakiris, U. Schramm, T.P. Rowlands-Rees, S.M. Hooker, D. Habs, F. Krausz, S. Karsch, F. Grüner, Nat. Phys. 5 (2009) 826.

[177] J.H. Han, H.S. Kang, I.S. Ko, Proceedings of IPAC2012, New Orleans, Louisiana, USA, 2012.
[178] B.D. Patterson, R. Abela, PCCP 12 (2010) 5647.
[179] B.D. Patterson, R. Abela, H.-H. Braun, U. Flechsig, R. Ganter, Y. Kim, E. Kirk, A. Oppelt, M. Pedrozzi, S. Reiche, L. Rivkin, T. Schmidt, B. Schmitt, V.N. Strocov, S. Tsujino, A.F. Wrulich, New J. Phys. 12 (2010) 035012.
[180] V. Wacker, Y. Ding, J. Frisch, Z. Huang, C. Pellegrini, F. Zhou, FEL 2012-34th International Free Electron Laser Conference, 2012, p. 606.
[181] Y. Feng, J.M. Feldkamp, D.M. Fritz, M. Cammarata, A. Robert, C. Caronna, H.T. Lemke, D. Zhu, S. Lee, S. Boutet, G. Williams, K. Tono, M. Yabashi, J.B. Hastings, Proceedings of SPIE – The International Society for Optical Engineering, 2011.
[182] K. Tono, T. Kudo, M. Yabashi, T. Tachibana, Y. Feng, D. Fritz, J. Hastings, T. Ishikawa, Rev. Sci. Instrum. 82 (2011) 023108.
[183] R. Alonso-Mori, J. Kern, R.J. Gildea, D. Sokaras, T.C. Weng, B. Lassalle-Kaiser, R. Tran, J. Hattne, H. Laksmono, J. Hellmich, C. Glockner, N. Echols, R.G. Sierra, D.W. Schafer, J. Sellberg, C. Kenney, R. Herbst, J. Pines, P. Hart, S. Herrmann, R.W. Grosse-Kunstleve, M.J. Latimer, A.R. Fry, M.M. Messerschmidt, A. Miahnahri, M.M. Seibert, P.H. Zwart, W.E. White, P.D. Adams, M.J. Bogan, S. Boutet, G.J. Williams, A. Zouni, J. Messinger, P. Glatzel, N.K. Sauter, V.K. Yachandra, J. Yano, U. Bergmann, Proc. Natl. Acad. Sci. U.S.A. 109 (2012) 19103.
[184] J. Kern, R. Alonso-Mori, R. Tran, J. Hattne, R.J. Gildea, N. Echols, C. Glockner, J. Hellmich, H. Laksmono, R.G. Sierra, B. Lassalle-Kaiser, S. Koroidov, A. Lampe, G. Han, S. Gul, D. DiFiore, D. Milathianaki, A.R. Fry, A. Miahnahri, D.W. Schafer, M. Messerschmidt, M.M. Seibert, J.E. Koglin, D. Sokaras, T.C. Weng, J. Sellberg, M.J. Latimer, R.W. Grosse-Kunstleve, P.H. Zwart, W.E. White, P. Glatzel, P.D. Adams, M.J. Bogan, G.J. Williams, S. Boutet, J. Messinger, A. Zouni, N.K. Sauter, V.K. Yachandra, U. Bergmann, J. Yano, Science 340 (2013) 491.
[185] J. Szlachetko, C.J. Milne, J. Hoszowska, J-Cl. Dousse, W. Błachucki, J. Sà, Y. Kayser, M. Messerschmidt, R. Abela, S. Boutet, C. David, G. Williams, M. Pajek, B.D. Patterson, G. Smolentsev, J. A. van Bokhoven, M. Nachtegaal, Struc. Dyn. (in press).
[186] D. Zhu, M. Cammarata, J.M. Feldkamp, D.M. Fritz, J.B. Hastings, S. Lee, H.T. Lemke, A. Robert, J.L. Turner, Y. Feng, Appl. Phys. Lett. 101 (2012) 034103.
[187] G. Geloni, V. Kocharyan, E. Saldin, J Mod. Optics 58 (2011) 1391.
[188] J. Amann, W. Berg, V. Blank, F.J. Decker, Y. Ding, P. Emma, Y. Feng, J. Frisch, D. Fritz, J. Hastings, Nat. Photonics 6 (2012) 693.
[189] E. Allaria, C. Callegari, D. Cocco, W.M. Fawley, M. Kiskinova, C. Masciovecchio, F. Parmigiani, New J. Phys. 12 (2010) 075002.
[190] Y. Feng, D. Zhu, A. Robert, H.T. Lemke, M. Chollet, D.M. Fritz, J.B. Hastings, J.M. Feldkamp, M. Cammarata, S. Moeller, M. Yabashi, K. Tono, X. Huang, in: S.P. Moeller, M. Yabashi, S.P. Hau-Riege (Eds.), SPIE Optical Engineering + Applications, SPIE, 2012, pp. 85040–85046.
[191] D. Mills, A. Lewis, A. Harootunian, J. Huang, B. Smith, Science 223 (1984) 811.
[192] D.M. Mills, Phys. Today (1984) 22.
[193] G. Jennings, W. Jager, L.X. Chen, Rev. Sci. Instrum. 73 (2002) 362.
[194] M. Cammarata, L. Eybert, F. Ewald, W. Reichenbach, M. Wulff, P.A. Anfinrud, F. Schotte, A. Plech, Q. Kong, M. Lorenc, B. Lindenau, J. Raebiger, S. Polachowski, Rev. Sci. Instrum. 80 (2009) 015101.
[195] L.X. Chen, X. Zhang, E.C. Wasinger, K. Attenkofer, G. Jennings, A.Z. Muresan, J.S. Lindsey, J. Am. Chem. Soc. 129 (2007) 9616.
[196] F. Lima, C. Milne, D. Amarasinghe, M. Rittmann-Frank, R. van der Veen, M. Reinhard, V. Pham, S. Karlsson, S. Johnson, D. Grolimund, C. Borca, T. Huthwelker, M. Janousch, F. van Mourik, R. Abela, M. Chergui, Rev. Sci. Instrum. 82 (2011) 063111.
[197] A.M. March, A. Stickrath, G. Doumy, E.P. Kanter, B. Krässig, S.H. Southworth, K. Attenkofer, C.A. Kurtz, L.X. Chen, L. Young, Rev. Sci. Instrum. 82 (2011) 073110.
[198] L. Stebel, M. Malvestuto, V. Capogrosso, P. Sigalotti, B. Ressel, F. Bondino, E. Magnano, G. Cautero, F. Parmigiani, Rev. Sci. Instrum. 82 (2011) 123109.
[199] K. Haldrup, G. Vankó, W. Gawelda, A. Galler, G. Doumy, A.M. March, E.P. Kanter, A. Bordage, A. Dohn, T.B. van Driel, K.S. Kjær, H.T. Lemke, S.E. Canton, J. Uhlig, V. Sundstrom, L. Young, S.H. Southworth, M.M. Nielsen, C. Bressler, J. Phys. Chem. A 116 (2012) 9878.
[200] G. Capano, T.J. Penfold, N.A. Besley, C.J. Milne, M. Reinhard, H. Rittmann-Frank, P. Glatzel, R. Abela, U. Rothlisberger, M. Chergui, I. Tavernelli, Chem. Phys. Lett. 580 (2013) 179.
[201] A. El Nahhas, R.M. van der Veen, T.J. Penfold, V.T. Pham, F.A. Lima, R. Abela, A.M. Blanco-Rodriguez, S. Zalis, A. Vlcek, I. Tavernelli, U. Rothlisberger, C.J. Milne, M. Chergui, J. Phys. Chem. A 117 (2013) 361.
[202] S. Zalis, C.J. Milne, A. el Nahhas, A.M. Blanco-Rodriguez, R.M. van der Veen, A. Vlček Jr., Inorg. Chem. 52 (2013) 5775.
[203] T.J. Penfold, S. Karlsson, G. Capano, F.A. Lima, J. Rittmann, M. Reinhard, M.H. Rittmann-Frank, O. Braem, E. Baranoff, R. Abela, I. Tavernelli, U. Rothlisberger, C.J. Milne, M. Chergui, J. Phys. Chem. A 117 (2013) 4591.
[204] M. Rittmann-Frank, C. Milne, J. Rittmann, M. Reinhard, T. Penfold, M. Chergui, Angewandte Chemie International Edition (in press).
[205] A. Cannizzo, A. Blanco-Rodríguez, A. el Nahhas, J. Šebera, S. Zalis, A. Vlček Jr., M. Chergui, J. Am. Chem. Soc. 130 (2008) 8967.
[206] A. el Nahhas, A. Cannizzo, F. van Mourik, A.M. Blanco-Rodriguez, S. Zalis, A.J. Vlcek, M. Chergui, J. Phys. Chem. A 114 (2010) 6361.
[207] D.R. McMillin, J.R. Kirchhoff, K.V. Goodwin, Coord. Chem. Rev. 64 (1985) 83.
[208] G.B. Shaw, C.D. Grant, H. Shirota, E.W. CASTNER, G.J. Meyer, L.X. Chen, J. Am. Chem. Soc. 129 (2007) 2147.
[209] G. Smolentsev, A.V. Soldatov, L.X. Chen, J. Phys. Chem. A 112 (2008) 5363.
[210] G. Vanko, P. Glatzel, V.-T. Pham, R. Abela, D. Grolimund, C.N. Borca, S.L. Johnson, C.J. Milne, C. Bressler, Angew. Chem. Int. Ed. 49 (2010) 5910.
[211] G. Vankó, A. Bordage, P. Glatzel, E. Gallo, M. Rovezzi, W. Gawelda, A. Galler, C. Bressler, G. Doumy, A.M. March, E.P. Kanter, L. Young, S.H. Southworth, S.E. Canton, J. Uhlig, G. Smolentsev, V. Sundstrom, K. Haldrup, T.B. van Driel, M.M. Nielsen, K.S. Kjær, H.T. Lemke, J. Electron Spectrosc. Relat. Phenom. 188 (2013) 166.
[212] B. Van Kuiken, M. Khalil, J. Phys. Chem. A 115 (2011) 10749.
[213] M. Pápai, G. Vanko, C. de Graaf, T. Rozgonyi, J. Chem. Theory Comput. 9 (2013) 509.
[214] P. Beaud, S.L. Johnson, E. Vorobeva, U. Staub, R.A. de Souza, C.J. Milne, Q.X. Jia, G. Ingold, Phys. Rev. Lett. 103 (2009) 155702.
[215] S. Johnson, P. Beaud, E. Vorobeva, C. Milne, E. Murray, S. Fahy, G. Ingold, Phys. Rev. Lett. 102 (2009) 175503.
[216] S. Johnson, E. Vorobeva, P. Beaud, C. Milne, G. Ingold, Phys. Rev. Lett. 103 (2009) 205501.
[217] S.L. Johnson, P. Beaud, C.J. Milne, F.S. Krasniqi, E.S. Zijlstra, M.E. Garcia, M. Kaiser, D. Grolimund, R. Abela, G. Ingold, Phys. Rev. Lett. 100 (2008) 155501.
[218] F.S. Krasniqi, S.L. Johnson, P. Beaud, M. Kaiser, D. Grolimund, G. Ingold, Phys. Rev. B 78 (2008) 174302.
[219] S. Mariager, F. Pressacco, G. Ingold, A. Caviezel, E. Möhr-Vorobeva, P. Beaud, S. Johnson, C. Milne, E. Mancini, S. Moyerman, E. Fullerton, R. Feidenhans'l, C. Back, C. Quitmann, Phys. Rev. Lett. 108 (2012) 087201.
[220] A. Caviezel, U. Staub, S. Johnson, S. Mariager, E. Möhr-Vorobeva, G. Ingold, C. Milne, M. Garganourakis, V. Scagnoli, S. Huang, Q. Jia, S.W. Cheong, P. Beaud, Phys. Rev. B 86 (2012) 174105.
[221] E. Moehr-Vorobeva, S.L. Johnson, P. Beaud, U. Staub, R. De Souza, C. Milne, G. Ingold, J. Demsar, H. Schaefer, A. Titov, Phys. Rev. Lett. 107 (2011) 036403.
[222] B. Mansart, M.J.G. Cottet, G.F. Mancini, T. Jarlborg, S.B. Dugdale, S.L. Johnson, S.O. Mariager, C.J. Milne, P. Beaud, S. Grübel, J.A. Johnson, T. Kubacka, G. Ingold, K. Prsa, H.M. Rønnow, K. Conder, E. Pomjakushina, M. Chergui, F. Carbone, Phys. Rev. B 88 (2013) 054507.
[223] C.J. Milne, V.-T. Pham, W. Gawelda, R.M. van der Veen, A. el Nahhas, S.L. Johnson, P. Beaud, G. Ingold, F.A. Lima, D.A. Vithanage, M. Benfatto, D. Grolimund, C.N. Borca, M. Kaiser, A. Hauser, R. Abela, C. Bressler, M. Chergui, JPCS 190 (2009) 012052.
[224] T.J. Penfold, C.J. Milne, I. Tavernelli, M. Chergui, Pure Appl. Chem. 85 (2013) 53.
[225] T. Penfold, I. Tavernelli, M. Doemer, R. Abela, U. Röthlisberger, M. Chergui, Chem. Phys. 410 (2013) 25.
[226] A. Cavalleri, M. Rini, H. Chong, S. Fourmaux, T. Glover, P. Heimann, J. Kieffer, R. Schoenlein, Phys. Rev. Lett. 95 (2005) 067405.
[227] H. Wen, N. Huse, R.W. Schoenlein, A.M. Lindenberg, J. Chem. Phys. 131 (2009) 234505.
[228] N. Huse, H. Wen, D. Nordlund, E. Szilagyi, D. Daranciang, T.A. Miller, A. Nilsson, R.W. Schoenlein, A.M. Lindenberg, PCCP 11 (2009) 3951.
[229] P. Wernet, G. Gavrila, K. Godehusen, C. Weniger, E.T.J. Nibbering, T. Elsaesser, W. Eberhardt, Appl. Phys. A: Mater. Sci. 92 (2008) 511.
[230] G. Gavrila, K. Godehusen, C. Weniger, E.T.J. Nibbering, T. Elsaesser, W. Eberhardt, P. Wernet, Appl. Phys. A Mater. Sci. 96 (2009) 11.
[231] P. Wernet, JPCS 190 (2009) 012055.
[232] H. Cho, M.L. Strader, K. Hong, L. Jamula, E.M. Gullikson, T.K. Kim, F.M.F. de Groot, J.K. McCusker, R.W. Schoenlein, N. Huse, Faraday Discuss. 157 (2012) 463.
[233] C. Stamm, T. Kachel, N. Pontius, R. Mitzner, T. Quast, K. Holldack, S. Khan, C. Lupulescu, E.F. Aziz, M. Wietstruk, H.A. Durr, W. Eberhardt, Nat. Mater. 6 (2007) 740.
[234] C. Stamm, N. Pontius, T. Kachel, M. Wietstruk, H.A. Durr, Phys. Rev. B 81 (2010) 104425.
[235] K. Holldack, N. Pontius, E. Schierle, T. Kachel, V. Soltwisch, R. Mitzner, T. Quast, G. Springholz, E. Weschke, Appl. Phys. Lett. 97 (2010) 062502.
[236] C. Boeglin, E. Beaurepaire, V. Halté, V. López-Flores, C. Stamm, N. Pontius, H.A. Durr, J.Y. Bigot, Nature 465 (2010) 458.
[237] I. Radu, K. Vahaplar, C. Stamm, T. Kachel, N. Pontius, H.A. Durr, T.A. Ostler, J. Barker, R.F.L. Evans, R.W. Chantrell, A. Tsukamoto, A. Itoh, A. Kirilyuk, T. Rasing, A.V. Kimel, Nature 472 (2011) 205.
[238] S. Boutet, L. Lomb, G.J. Williams, T.R.M. Barends, A. Aquila, R.B. Doak, U. Weierstall, D.P. DePonte, J. Steinbrener, R.L. Shoeman, M. Messerschmidt, A. Barty, T.A. White, S. Kassemeyer, R.A. Kirian, M.M. Seibert, P.A. Montanez, C. Kenney, R. Herbst, P. Hart, J. Pines, G. Haller, S.M. Gruner, H.T. Philipp, M.W. Tate, M. Hromalik, L.J. Koerner, N. van Bakel, J. Morse, W. Ghonsalves, D. Arnlund, M.J. Bogan, C. Caleman, R. Fromme, C.Y. Hampton, M.S. Hunter, L.C. Johansson, G. Katona, C. Kupitz, M. Liang, A.V. Martin, K. Nass, L. Redecke, F. Stellato, N. Timneanu, D. Wang, N.A. Zatsepin, D. Schafer, J. Defever, R. Neutze, P. Fromme, J.C.H. Spence, H.N. Chapman, I. SCHLICHTING, Science 337 (2012) 362.
[239] J.C.H. Spence, U. Weierstall, H.N. Chapman, Rep. Prog. Phys. 75 (2012) 102601.
[240] A. Barty, J. Küpper, H.N. Chapman, Annu. Rev. Phys. Chem. 64 (2013) 415.
[241] L. Young, E.P. Kanter, B. Krässig, Y. Li, A.M. March, S.T. Pratt, R. Santra, S.H. Southworth, N. Rohringer, L.F. Dimauro, G. Doumy, C.A. Roedig, N. Berrah, L. Fang, M. Hoener, P.H. Bucksbaum, J.P. Cryan, S. Ghimire, J.M. Glownia, D.A. Reis, J.D. Bozek, C. Bostedt, M. Messerschmidt, Nature 466 (2010) 56.
[242] M.R. Bionta, H.T. Lemke, J.P. Cryan, J.M. Glownia, C. Bostedt, M. Cammarata, J.C. Castagna, Y. Ding, D.M. Fritz, A.R. Fry, J. Krzywinski, M. Messerschmidt, S. Schorb, M. Swiggers, R. Coffee, Opt. Express 19 (2011) 21855.
[243] O. Krupin, M. Trigo, W.F. Schlotter, M. Beye, F. Sorgenfrei, J.J. Turner, D.A. Reis, N. Gerken, S. Lee, W.S. Lee, G. Hays, Y. Acremann, B. Abbey, R. Coffee, M. Messerschmidt, S. Hau-Riege, G. Lapertot, J. Luning, P. Heimann, R. Soufli,

M. Fernandez-Perea, M. Rowen, M. Holmes, S.L. Molodtsov, A. Foehlisch, W. Wurth, Opt. Express 20 (2012) 11396.
[244] C. Consani, M. Prémont-Schwarz, A. ElNahhas, C. Bressler, F. van Mourik, A. Cannizzo, M. Chergui, Angew. Chem. Int. Ed. 48 (2009) 7184.
[245] T.J. Penfold, I. Tavernelli, R. Abela, M. Chergui, U. Rothlisberger, New J. Phys. 14 (2012) 113002.
[246] G. Dixit, O. Vendrell, R. Santra, Proc. Natl. Acad. Sci. U.S.A. 109 (2012) 11636.
[247] G. Dixit, R. Santra, J. Chem. Phys. 138 (2013) 134311.
[248] B. Pedrini, A. Menzel, M. Guizar-Sicairos, V.A. Guzenko, S. Gorelick, C. David, B.D. Patterson, R. Abela, Nature Comm. 4 (2013) 1647.
[249] B. Patterson, Resource letter on stimulated inelastic X-ray scattering at an xfel, see http://slac.stanford.edu/pubs/slactns/tn04/slac-tn-10-026.pdf, Technical Report 2010.
[250] N. Rohringer, D. Ryan, R.A. London, M. Purvis, F. Albert, J. Dunn, J.D. Bozek, C. Bostedt, A. Graf, R. Hill, S.P. Hau-Riege, J.J. Rocca, Nature 481 (2012) 488.
[251] M. Beye, S. Schreck, F. Sorgenfrei, C. Trabant, N. Pontius, C. Schüßler-Langeheine, W. Wurth, A. Föhlisch, Nature 501 (2013) 191.
[252] S. Tanaka, V. Chernyak, S. Mukamel, Phys. Rev. A 63 (2001) 063405.
[253] S. Tanaka, S. Mukamel, Phys. Rev. Lett. 89 (2002) 043001.
[254] S. Tanaka, S. Mukamel, J. Chem. Phys. 116 (2002) 1877.
[255] F. Bencivenga, S. Baroni, C. Carbone, M. Chergui, M.B. Danailov, G. de Ninno, M. Kiskinova, L. Raimondi, C. Svetina, C. Masciovecchio, New J. Phys. 15 (2013) 123023.
[256] J. Rehr, R. Albers, Phys. Rev. B 41 (1990) 8139.
[257] C. Natoli, M. Benfatto, C. Brouder, M. Ruiz Lopez, D. Foulis, Phys. Rev. B 42 (1990) 1.
[258] J. Rehr, R. Albers, S. Zabinsky, Phys. Rev. Lett. 69 (1992) 3397.
[259] J. Rehr, A. Ankudinov, Coord. Chem. Rev. 249 (2005) 131.
[260] F.M.F. de Groot, J. Electron, Spectrosc. Relat. Phenom. 67 (1994) 529.
[261] R. Cowan, The Theory of Atomic Structure and Spectra, University of California Press, Berkeley and Los Angeles, 1981.
[262] F. de Groot, J.C. Fuggle, B.T. Thole, G.A. Sawatzky, Phys. Rev. B 42 (1990) 5459.
[263] Y. Joly, Phys. Rev. B 63 (2001) 125120.
[264] M. Benfatto, A. Congiu-Castellano, A. Daniele, S. Longa, J Synchrotron Radiat. 267 (2014).
[265] J. Rehr, J. Kas, F. Vila, M. Prange, K. Jorissen, PCCP 12 (2010) 5503.
[266] K. Schwarz, P. Blaha, Mol. Phys. 108 (2010) 21.
[267] E. Gaudry, D. Cabaret, P. Sainctavit, C. Brouder, F. Mauri, J. Goulon, A. Rogalev, J. Phys.: Condens. Matter 17 (2005) 5467.
[268] X. Gonze, B. Amadon, P.M. Anglade, Comput. Phys. Commun. 180 (2009) 2582.
[269] M. Taillefumier, D. Cabaret, A.M. Flank, F. Mauri, Phys. Rev. B 66 (2002) 195107.
[270] F. Neese, WIREs Comput. Mol. Sci. 2 (2012) 73.
[271] G. Te Velde, F. Bickelhaupt, Chemistry, Weinheim an der Bergstrasse, Germany, 2001.
[272] C. Kolczewski, K. Hermann, Theor. Chem. Acc. 114 (2005) 60.
[273] E. Stavitski, F. de Groot, Micron 41 (2010) 687.
[274] A. Uldry, F. Vernay, B. Delley, Phys. Rev. B 85 (2012) 125133.
[275] N. Papanikolaou, R. Zeller, P.H. Dederichs, J. Phys.: Condens. Matter 14 (2002) 2799.
[276] J.B. Danese, J. Chem. Phys. Physics 61 (1974) 3071.
[277] J.B. Danese, J. Connolly, J. Chem. Phys. 61 (1974) 3063.
[278] P. Lloyd, P.V. Smith, Adv. Phys. 21 (1972) 69.
[279] A.R. Williams, J. van, W. Morgan, J. Phys. C 7 (1974) 37.
[280] C. Natoli, M. Benfatto, S. Doniach, Phys. Rev. A 34 (1986) 4682.
[281] D.L. Foulis, R.F. Pettifer, C.R. Natoli, M. Benfatto, Phys. Rev. A 41 (1990) 6922.
[282] A.L. Ankudinov, J. Rehr, Phys. Scr. (2005) 24.
[283] K. Hatada, K. Hayakawa, M. Benfatto, C. Natoli, Phys. Rev. B 76 (2007) 060102.
[284] K. Hatada, K. Hayakawa, M. Benfatto, C. Natoli, J. Phys.: Condens. Matter 22 (2010) 185501.
[285] Y. Joly, Phys. Rev. B 53 (1996) 13029.
[286] C. Witte, C. Chantler, E. Cosgriff, C. Tran, Radiat. Phys. Chem. 75 (2006) 1582.
[287] L. Triguero, L. Pettersson, H. Ågren, Phys. Rev. B 58 (1998) 8097.
[288] O. Bunău, M. Calandra, Phys. Rev. B 87 (2013) 205105.
[289] J. Vinson, J.J. Rehr, J.J. Kas, E.L. Shirley, Phys. Rev. B 83 (2011) 115106.
[290] P.E. Blöchl, Phys. Rev. B 50 (1994) 17953.
[291] G. Lippert, J. Hutter, M. Parrinello, Theor. Chem. Acc. 103 (1999) 124.
[292] CP2K a general program to perform molecular dynamics simulations. http://cp2k.berlios.de, 2006.
[293] M. Iannuzzi, J. Chem. Phys. 128 (2008) 204506.
[294] M. Iannuzzi, J. Hutter, PCCP 9 (2007) 1599.
[295] E. Runge, E. Gross, Phys. Rev. Lett. 52 (1984) 997.
[296] M. Casida, M. Huix-Rotllant, Annu. Rev. Phys. Chem. 63 (2012) 287.
[297] C. Ullrich, Time-Dependent Density-Functional Theory, Oxford Graduate Texts, Oxford, 2011.
[298] A. Zangwill, P. Soven, Phys. Rev. A 21 (1980) 1561.
[299] A. Ankudinov, A. Nesvizhskii, J. Rehr, Phys. Rev. B 67 (2003) 115120.
[300] O. Bunău, Y. Joly, J. Phys.: Condens. Matter 24 (2012) 215502.
[301] Y. Shao, L.F. Molnar, Y. Jung, r. Kussmann, C. Ochsenfeld, S.T. Brown, A.T.B. Gilbert, L.V. Slipchenko, S.V. Levchenko, D.P.O. Neill, R.A. DiStasio Jr., R.C. Lochan, T. Wang, G.J.O. Beran, N.A. Besley, J.M. Herbert, C. Yeh Lin, T. Van Voorhis, S. Hung Chien, A. Sodt, R.P. Steele, V.A. Rassolov, P.E. Maslen, P.P. Korambath, R.D. Adamson, B. Austin, J. Baker, E.F.C. Byrd, H. Dachsel, R.J. Doerksen, A. Dreuw, B.D. Dunietz, A.D. Dutoi, T.R. Furlani, S.R. Gwaltney, A. Heyden, S. Hirata, C.-P. Hsu, G. Kedziora, R.Z. Khalliulin, P. Klunzinger, A.M. Lee, M.S. Lee, W. Liang, I. Lotan, N. Nair, B. Peters, E.I. Proynov, P.A. Pieniazek, Y. Min Rhee, J. Ritchie, E. Rosta, C. David Sherrill, A.C. Simmonett, J.E. Subotnik, H. Lee Woodcock III, W. Zhang, A.T. Bell, A.K. Chakraborty, D.M. Chipman, F.J. Keil, A. Warshel, W.J. Hehre, H.F. Schaefer III, J. Kong, A.I. Krylov, P.M.W. Gill, M. Head-Gordon, PCCP 8 (2006) 3172.
[302] M. Valiev, E.J. Bylaska, N. Govind, K. Kowalski, T.P. Straatsma, H.J. Van Dam, D. Wang, J. Nieplocha, E. Apra, T.L. Windus, Comput. Phys. Commun. 181 (2010) 1477.
[303] K. Lopata, B.E. Van Kuiken, M. Khalil, N. Govind, J. Chem. Theory Comput. 8 (2012) 3284.
[304] A. Lee, F. Vila, J. Rehr, Phys. Rev. B 86 (2012) 115107.
[305] A. Dreuw, M. Head-Gordon, Chem. Rev. 105 (2005) 4009.
[306] S. Hirata, M. Head-Gordon, Chem. Phys. Lett. 314 (1999) 291.
[307] M. Stener, Chem. Phys. Lett. 373 (2003) 115.
[308] S.D. George, T. Petrenko, F. Neese, J. Phys. Chem. A 112 (2008) 12936.
[309] N.A. Besley, A. Noble, J. Phys. Chem. C 111 (2007) 3333.
[310] M. Roemelt, M.A. Beckwith, C. Duboc, M.-N. Collomb, F. Neese, S. DeBeer, Inorg. Chem. 51 (2012) 680.
[311] S. DeBeer George, T. Petrenko, F. Neese, Inorg. Chim. Acta 361 (2008) 965.
[312] S.D. George, F. Neese, Inorg. Chem. 49 (2010) 1849.
[313] A.J. Atkins, M. Bauer, C.R. Jacob, PCCP 15 (2013) 8095.
[314] A.J. Atkins, C.R. Jacob, M. Bauer, Chem. Eur. J. 18 (2012) 7021.
[315] A. Nardelli, G. Fronzoni, M. Stener, J. Phys. Chem. C 113 (2009) 14844.
[316] G. Fronzoni, R. De Francesco, M. Stener, J. Phys. Chem. B 109 (2005) 10332.
[317] F.A. Lima, T.J. Penfold, R.M. van der Veen, M. Reinhard, R. abela, I. Tavernelli, U. Rothlisberger, M. Benfatto, C.J. milne, M. chergui, PCCP 16 (2014) 1617.
[318] A. Dreuw, J. Weisman, M. Head-Gordon, J. Chem. Phys. 119 (2003) 2943.
[319] M. Roemelt, M. Beckwith, C. Duboc, M. Collomb, F. Neese, S. DeBeer, Inorg. Chem. 51 (2012) 680.
[320] R. Van Leeuwen, E.J. Baerends, Phys. Rev. A 49 (1994) 2421.
[321] S. Debeer-George, T. Petrenko, F. Neese, Inorg. Chim. Acta 361 (2008) 965.
[322] J.W. Song, S. Tokura, T. Sato, M.A. Watson, K. Hirao, J. Chem. Phys. 127 (2007) 154109.
[323] N. Besley, M. Peach, D. Tozer, PCCP 11 (2009) 10350.
[324] M. Nooijen, R. Bartlett, J. Chem. Phys. 102 (1995) 6735.
[325] N.A. Besley, Chem. Phys. Lett. 542 (2012) 42.
[326] J. Brabec, K. Bhaskaran-Nair, N. Govind, J. Pittner, K. Kowalski, J. Chem. Phys. 137 (2012) 171101.
[327] J. Schirmer, Phys. Rev. A 26 (1982) 2395.
[328] I. Bâldea, B. Schimmelpfennig, M. Plaschke, J. Rothe, J. Schirmer, A.B. Trofimov, T. Fanghänel, J. Electron Spectrosc. Relat. Phenom. 154 (2007) 109.
[329] O. Plekan, V. Feyer, R. Richter, M. Coreno, M. de Simone, K.C. Prince, A.B. Trofimov, E.V. Gromov, I.L. Zaytseva, J. Schirmer, Chem. Phys. 347 (2008) 360.
[330] V. Feyer, O. Plekan, R. Richter, M. Coreno, M. de Simone, K.C. Prince, A.B. Trofimov, I.L. Zaytseva, J. Schirmer, J. Phys. Chem. A 114 (2010) 10270.
[331] O. Plekan, V. Feyer, R. Richter, M. Coreno, G. Vall-llosera, K.C. Prince, A.B. Trofimov, I.L. Zaytseva, T.E. Moskovskaya, E.V. Gromov, J. Schirmer, J. Phys. Chem. A 113 (2009) 9376.
[332] F. Asmuruf, N. Besley, Chem. Phys. Lett. 463 (2008) 267–271.
[333] M. Roemelt, D. Maganas, S. DeBeer, F. Neese, J. Chem. Phys. 138 (2013) 204101.
[334] H. Ikeno, F.M.F. de Groot, E. Stavitski, I. Tanaka, J. Phys.: Condens. Matter 21 (2009) 104208.
[335] F. Neese, T. Petrenko, D. Ganyushin, G. Olbrich, Coord. Chem. Rev. 251 (2007) 288.
[336] S. Grimme, Chem. Phys. Lett. 259 (1996) 128.
[337] S. Grimme, M. Waletzke, J. Chem. Phys. 111 (1999) 5645.
[338] D. Maganas, M. Roemelt, M. Hävecker, A. Trunschke, A. Knop-Gericke, R. Schlögl, F. Neese, PCCP 15 (2013) 7260.
[339] D. Maganas, M. Roemelt, T. Weyhermuller, R. Blume, M. Haevecker, A. Knop-Gericke, S. DeBeer, R. Schlogl, F. Neese, PCCP 16 (2014) 264.
[340] M.W. Schmidt, M.S. Gordon, Annu. Rev. Phys. Chem. 49 (1998) 233.
[341] B.O. Roos, K. Andersson, M.P. Fülscher, P.-Å. Malmqvist, L. Serrano-Andrés, K. Pierloot, M. Merchán, Adv. Chem. Phys. 93 (1996) 219.
[342] S.I. Bokarev, M. Dantz, E. Suljoti, O. Kühn, E.F. Aziz, Phys. Rev. Lett. 111 (2013) 083002.
[343] K. Atak, S.I. Bokarev, M. Gotz, R. Golnak, K.M. Lange, N. Engel, M. Dantz, E. Suljoti, O. Kühn, E.F. Aziz, J. Phys. Chem. B 117 (2013) 12613.
[344] D.P. Tew, W. Klopper, T. Helgaker, J. Comput. Chem. 28 (2007) 1307.
[345] E.E. Salpeter, H.A. Bethe, Phys. Rev. 84 (1951) 1232–1242.
[346] L. Reining, V. Olevano, A. Rubio, G. Onida, Phys. Rev. Lett. 88 (2002) 066404.
[347] G. Onida, L. Reining, A. Rubio, Rev. Mod. Phys. 74 (2002) 601.
[348] J. Vinson, J. Rehr, Phys. Rev. B 86 (2012) 195135.
[349] E.L. Shirley, J. Electron Spectrosc. Relat. Phenom. 136 (2004) 77.
[350] E.L. Shirley, J. Electron Spectrosc. Relat. Phenom. 144–147 (2005) 1187.
[351] J. Vinson, J.J. Kas, F. Vila, J. Rehr, E.L. Shirley, Phys. Rev. B 85 (2012) 045101.
[352] D. Sayers, E. Stern, F. Lytle, Phys. Rev. Lett. 27 (1971) 1204.
[353] H. Funke, A. Scheinost, M. Chukalina, Phys. Rev. B 71 (2005) 094110.
[354] H. Funke, M. Chukalina, A.C. Scheinost, J. Synchrotron Radiat. 14 (2007) 426.
[355] D. Koningsberger, B. Mojet, G. Van Dorssen, D. Ramaker, Top. Catal. 10 (2000) 143.
[356] T.J. Penfold, I. Tavernelli, C.J. Milne, M. Reinhard, A.E. Nahhas, R. Abela, U. Rothlisberger, M. Chergui, J. Chem. Phys. 138 (2013) 014104.
[357] D. Manuel, D. Cabaret, C. Brouder, P. Sainctavit, A. Bordage, N. Trcera, Phys. Rev. B 85 (2012) 224108.
[358] P. D'Angelo, S. Della Longa, A. Arcovito, M. Anselmi, A. Di Nola, G. Chillemi, J. Am. Chem. Soc. 132 (2010) 14901.

[359] A. Tongraar, J. T-Thienprasert, S. Rujirawat, S. Limpijumnong, PCCP 12 (2010) 10876.
[360] V.T. Pham, I. Tavernelli, C.J. Milne, R.M. van der Veen, P. D'Angelo, C. Bressler, M. Chergui, Chem. Phys. 371 (2010) 24.
[361] T.J. Penfold, B.F.E. Curchod, I. Tavernelli, R. Abela, U. Rothlisberger, M. Chergui, PCCP 14 (2012) 9444.
[362] E.C. Beret, R.R. Pappalardo, D. Marx, E. Sánchez Marcos, Chemphyschem 10 (2009) 1044.
[363] E.C. Beret, K. Provost, D. Müller, E.S. Marcos, J. Phys. Chem. B 113 (2009) 12343.
[364] J.C. Tully, J. Chem. Phys. 93 (1990) 1061.
[365] M. Barbatti, WIREs Comput. Mol. Sci. 1 (2011) 620.
[366] B.F.E. Curchod, U. Rothlisberger, I. Tavernelli, ChemPhysChem 14 (2013) 1314.
[367] E. Tapavicza, I. Tavernelli, U. Rothlisberger, Phys. Rev. Lett. 98 (2007) 023001.
[368] E. Tapavicza, I. Tavernelli, U. Rothlisberger, C. Filippi, M.E. Casida, J. Chem. Phys. 129 (2008) 124108.
[369] I. Tavernelli, B.F.E. Curchod, U. Rothlisberger, J. Chem. Phys. 131 (2009) 196101.
[370] I. Tavernelli, B.F.E. Curchod, U. Rothlisberger, Phys. Rev. A 81 (2010) 052508.
[371] I. Tavernelli, B.F.E. Curchod, A. Laktionov, U. Rothlisberger, J. Chem. Phys. 133 (2010) 194104.
[372] I. Tavernelli, B.F. Curchod, U. Rothlisberger, Chem. Phys. 391 (2011) 101.
[373] B.F.E. Curchod, P. Campomanes, A. Laktionov, M. Neri, T.J. Penfold, S. Vanni, I. Tavernelli, U. Rothlisberger, Chimia 65 (2011) 330.
[374] A. Cannizzo, F. van Mourik, W. Gawelda, G. Zgrablic, C. Bressler, M. Chergui, Angew. Chem. Int. Ed. 45 (2006) 3174.
[375] C. Craig, W. Duncan, O. Prezhdo, Phys. Rev. Lett. 95 (2005) 163001.
[376] S.A. Fischer, B.F. Habenicht, A.B. Madrid, W.R. Duncan, O.V. Prezhdo, J. Chem. Phys. 134 (2011) 024102.
[377] A.V. Akimov, A.J. Neukirch, O.V. Prezhdo, Chem. Rev. 113 (2013) 4496.
[378] M.H. Beck, A. Jäckle, G.A. Worth, H.-D. Meyer, Phys. Rep. 324 (2000) 1.
[379] H.-D. Meyer, F. Gatti, G.A. Worth, High Dimensional Quantum Dynamics: Basic Theory, Extensions, and Applications of the MCTDH Method, VCH, Weinheim, Germany, 2008.
[380] H. Wang, M. Thoss, J. Chem. Phys. 119 (2003) 1289.
[381] O. Vendrell, H.-D. Meyer, J. Chem. Phys. 134 (2011) 044135.
[382] D. Mendive-Tapia, B. Lasorne, G. Worth, M.A. Robb, M.J. Bearpark, J. Chem. Phys. 137 (2012) 22A548.
[383] B. Lasorne, M. Robb, G. Worth, PCCP 9 (2007) 3210.
[384] A. Raab, G. Worth, H.-D. Meyer, L. Cederbaum, J. Chem. Phys. 110 (1999) 936.
[385] I. Kondov, M. Čížek, H. Benesch, M. Claudia ann d Wang, Thoss, J. Phys. Chem. C 111 (2007) 11970.
[386] J. Li, I. Kondov, H. Wang, M. Thoss, J. Phys. Chem. C 114 (2010) 18481.
[387] C. Weninger, N. Rohringer, Phys. Rev. A 88 (2013) 053421.
[388] D. Healion, H. Wang, S. Mukamel, J. Chem. Phys. 134 (2011) 1–2.
[389] J.D. Biggs, Y. Zhang, D. Healion, S. Mukamel, J. Chem. Phys. 136 (2012) 174117.
[390] Y. Zhang, J.D. Biggs, D. Healion, N. Govind, S. Mukamel, J. Chem. Phys. 137 (2012) 194306.
[391] W. Hua, J.D. Biggs, Y. Zhang, D. Healion, H. Ren, S. Mukamel, J. Chem. Theory Comput. 9 (2013) 5479.
[392] J.D. Biggs, Y. Zhang, D. Healion, S. Mukamel, Proc. Natl. Acad. Sci. U.S.A. 110 (2013) 15597.
[393] J.D. Biggs, Y. Zhang, D. Healion, S. Mukamel, J. Chem. Phys. 138 (2013) 144303.
[394] H. Navirian, R. Shayduk, W. Leitenberger, J. Goldshteyn, P. Gaal, M. Bargheer, Rev. Sci. Instrum. 83 (2012) 063303.